CALIFORNIA INSTITUTE OF TECHNOLOGY

EARTHQUAKE ENGINEERING RESEARCH LABORATORY

THE NONLINEAR RESPONSE OF SOME MULTISTORY REINFORCED AND PRESTRESSED CONCRETE STRUCTURES SUBJECTED TO EARTHQUAKE EXCITATION

by

Richard A. Spencer

A report on research conducted under a grant from the National Science Foundation

Pasadena, California

November 1968

THE NONLINEAR RESPONSE OF SOME MULTISTORY REINFORCED AND PRESTRESSED CONCRETE STRUCTURES SUBJECTED TO EARTHQUAKE EXCITATION

by R. A. Spencer

California Institute of Technology

November 1968

ACKNOWLEDGEMENTS

This study was supported by a grant from the National Science Foundation. Some of the computer programs used are similar to programs developed and written by M. F. Giberson.

The author is grateful for the assistance and advice given him by Professors G. W. Housner, D. E. Hudson, and P. C. Jennings.

ABSTRACT

The nonlinear dynamic responses of two reinforced and six prestressed concrete versions of a twenty story frame structure to a strong earthquake are found, using a step-by-step integration technique. A special model beam is used to represent the concrete members. The effects of different member properties, different amounts of hysteretic damping, and two different viscous damping mechanisms on response and energy dissipation are compared. The prestressed concrete structures have higher lateral displacements and inter-story drifts, but lower ductility requirements, and the comparative results suggest that a prestressed structure of the type analyzed could withstand a strong earthquake.

LIST OF SYMBOLS

A	Maximum story acceleration.
D_h	Hysteretic energy dissipation.
D_t	Total energy dissipation.
D_v	Total viscous energy dissipation.
D_{vi}	Interfloor viscous energy dissipation.
D_{vm}	Mass proportional viscous energy dissipation.
EI	Flexural rigidity.
F_c	Compressive force at the base of the exterior columns.
FR_h	Hinge flexural rigidity.
h	Hinge length factor.
K	Tridiagonal stiffness matrix.
K′	Full 20 x 20 stiffness matrix.
k	Stiffness factor for cracked hinge.
k_a	Stiffness factor for hinge at A.
k_b	Stiffness factor for hinge at B.
k_r	Hinge reversal stiffness factor.
L	Member length.
ℓ	Loopwidth factor.
M	Mass matrix
M_b	Base overturning moment.
M_c	Cracking moment.
M_e	End moment.
$M_f(x)$	Friction moment distribution.
M_h	Hinge moment.
$M_{h\ell}$	Width of $M_h - \theta_h$ loop.

LIST OF SYMBOLS (cont.)

M_{hr}	Total change in M_h when $M_h - \theta_h$ loop is crossed.
M_ℓ	Width of $M_e - \phi_e$ loop.
M_r	Total change in M_e when $M_e - \phi_e$ loop is crossed.
p	Member stiffness reduction factor for cracking.
p_r	Member stiffness factor for load reversal.
$\underline{U}$	Vector of story displacements relative to ground.
$\dot{\underline{U}}$	Vector of story velocities.
$\ddot{\underline{y}}$	Vector of absolute story accelerations.
α	Mass proportional viscous damping constant.
β	Interfloor viscous damping constant.
ξ_m	Mass proportional viscous damping factor.
ξ_i	Interfloor viscous damping factor.
θ_c	Hinge rotation when cracks just open.
θ_h	Hinge rotation.
μ_h	Hinge ductility factor.
μ_m	Member ductility factor.
ϕ_e	Member end rotation.

TABLE OF CONTENTS

1. INTRODUCTION

If prestressed concrete members are used as seismic resisting elements in tall frame structures, traditional static methods of design may not be suitable, because of the assumption, implicit in them, that the members can dissipate large amounts of energy by yielding. This is true for plain reinforced concrete members (1), but it is not normally the case when the members are prestressed (2). Thus, although confidence has been expressed (3) in the ability of certain types of prestressed concrete structure designed by conventional static methods to withstand strong earthquakes, there is a need for further investigation in the case of frame structures. In this paper the nonlinear dynamic responses of two reinforced and six prestressed concrete versions of a basic 20 story frame structure, designed by static load methods and subjected to a strong earthquake, are calculated and compared.

2. MEMBER MOMENT-ROTATION LOOPS

In order to make a rational, nonlinear, dynamic frame analysis, it is necessary to know the appropriate end moment-end rotation ($M_e - \phi_e$) hysteresis loops for the members. For prestressed concrete members the form of these loops is partly dependent on how the members are loaded, and the loops used here (shown in figure 1) to define the stiffness and damping properties of the prestressed members are for the special loading case of equal end moments applied in the same sense, as shown in figure 3a. These loops are idealized from loops which were found experimentally by applying this type of loading to a series of test members (2). The test moments varied cyclically about a mean of zero at frequencies of 0.5, 1.0 and 2.0 cycles/second, and because no

significant frequency dependent effects were observed, the idealized loops are also assumed to be frequency independent.

For this special loading case of equal end moments applied in the same sense, the member stiffness, S_1, when the cracks are closed by the prestress, is:

$$S_1 = 6EI/L \tag{1}$$

where EI is the appropriate flexural rigidity, and L is the loaded length. Each idealized loop can be completely described by S_1 and four other parameters defined as shown in figure 1:

The cracking moment, M_c, the end moment at which opening of the tension cracks causes the stiffness to fall;

the stiffness reduction factor, p, the ratio of the stiffness after cracking to S_1;

the reversal stiffness factor, p_r, the ratio of the stiffness when the loop is being crossed to S_1;

and the loopwidth factor, ℓ, the ratio of the loopwidth, M_ℓ, to M_c.

It is assumed that a load reversal can occur at any value of ϕ_e without changing the value of p_r. If a number of load reversals occur during a brief time interval, loading back and forth along the same reversal path can occur.

The common assumption is made here that reinforced concrete members can yield, and have $M_e - \phi_e$ loops like those shown in figure 2, with $p = 0.05$.

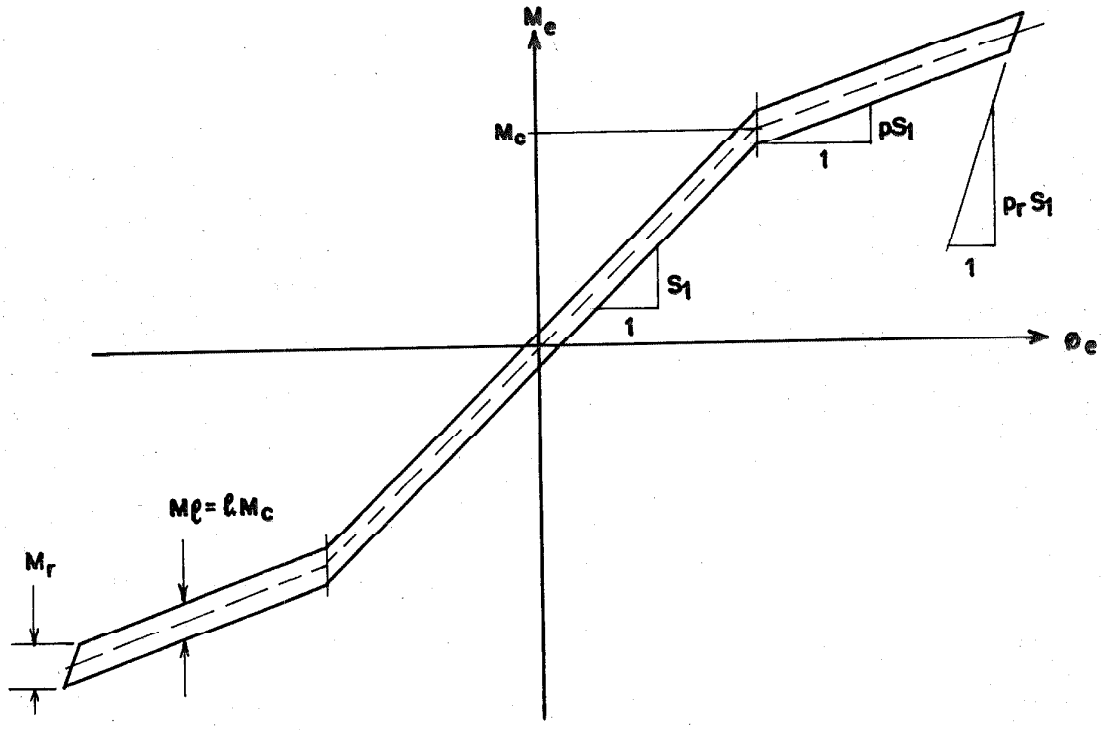

Figure 1: Typical M_e-ϕ_e hysteresis loop for prestressed concrete members.

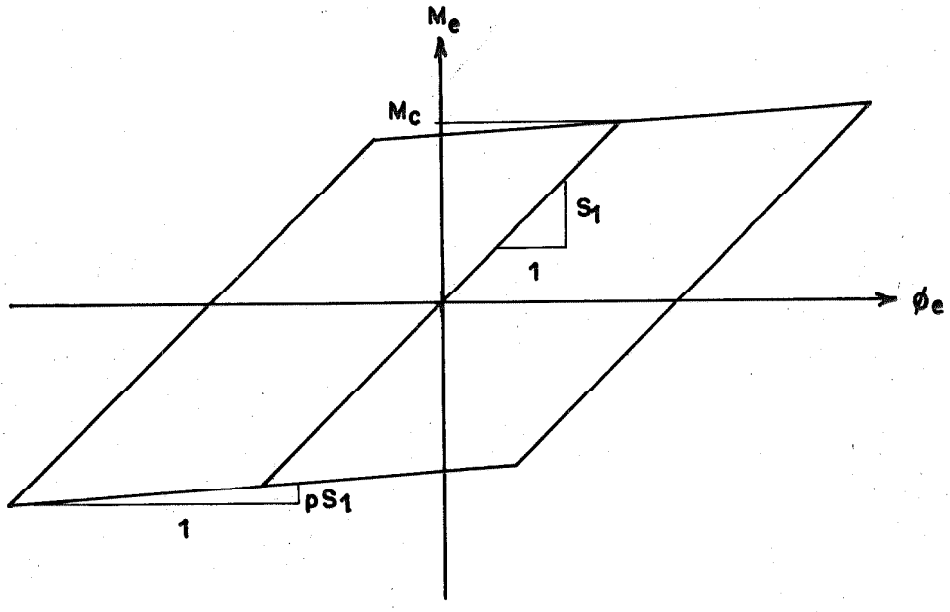

Figure 2: Typical M_e-ϕ_e hysteresis loop for reinforced concrete members

3. MODEL BEAMS

Each frame member is represented by a model beam, which has $M_e - \phi_e$ loops like those in either figure 1 or figure 2 for the special case shown in figure 3a. For each model beam, a hinge length factor, h , specifies a short, constant, hinge length, hL , at each end as shown in figure 3b. All cracking and energy dissipation in the beam is assumed to occur within these hinge lengths, and the central portion of the beam remains elastic, unaffected by either cracking or load reversal. A hinge length, rather than a simple hinge at a point, is chosen so that distress in the hinge, which depends on the hinge length factor ℓ and the value of p , can be estimated. The hinge length factors used in the analysis are based on observed values (1), (2), and it is assumed that the loading applied to the members during the response analysis does not vary sufficiently from that shown in figure 3a to make the assumption of a hinge of constant length unreasonable.

The hinge moment, M_h , or moment at the mid-point of the hinge, and the hinge rotation, θ_h , or angular change over the hinge length, are shown in figure 3b. For prestressed concrete members, an $M_h - \theta_h$ hysteresis loop like that shown in figure 3c is specified for each hinge length. The loop width is $M_{h\ell}$, and the hinge rotation when equal end moments M_c are applied as in figure 3a is θ_c . When the hinge rotation is less than θ_c , the hinge length is assumed to be uncracked, and its flexural rigidity, FR_h , is EI. When the hinge rotation exceeds θ_c, it is assumed that cracking within the hinge length has reduced its flexural rigidity to kEI . A load reversal in the hinge length, indicated by a change in the sign of $\dot{\theta}_h$, causes FR_h to rise to k_rEI until the

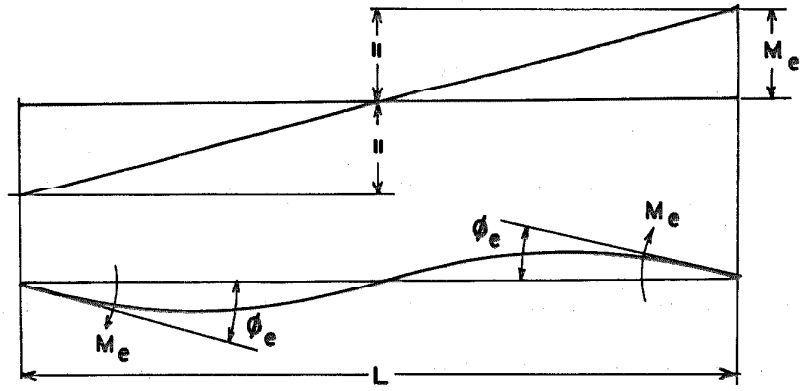

Figure 3a: Loading applied to test members

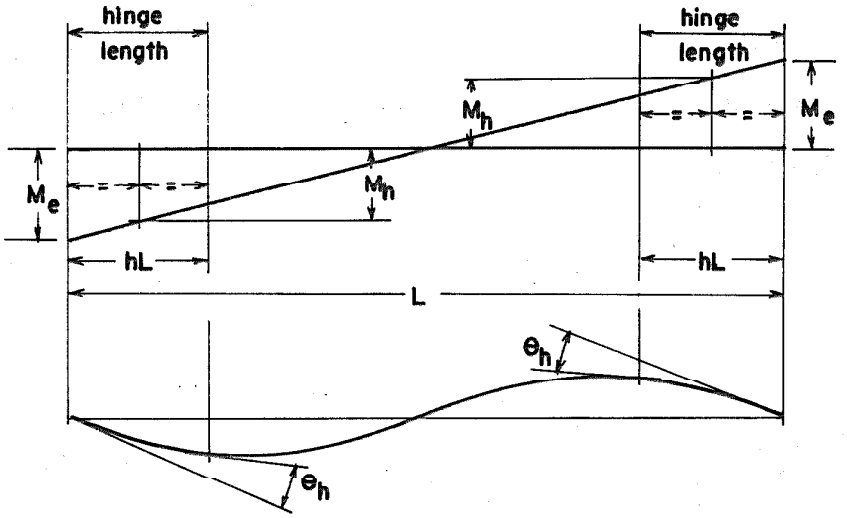

Figure 3b: M_h and θ_h defined

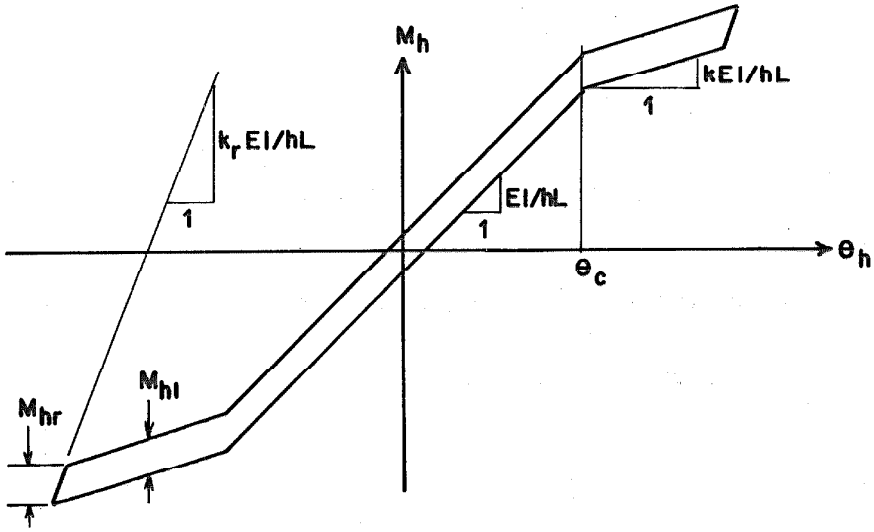

Figure 3c: Typical $M_h - \theta_h$ hysteresis loop for a prestressed hinge length.

$M_h - \theta_h$ loop is crossed. The assumption is made that like the hinge length, hL , the $M_h - \theta_h$ hysteresis loops do not vary during the response analysis.

To find the stiffness of a model beam like that shown in figure 4b, moments are applied separately at each end as shown in figure 4a. The stiffness reduction factors k_a and k_b shown in figure 4b can each have the value 1, k , or k_r depending on the hinge conditions, which may be different at each end. When the end moment applied at A is changed by ΔM_a , the corresponding changes in end-rotation are found, using Mohr's area-moment theorem, to be:

$$\Delta\phi_{aa} = \Delta M_a . K_1 . L/EI \tag{2}$$

where:

$$K_1 = \frac{1}{3}\left\{\begin{array}{l} 1 + \left(\frac{1}{k_a} - 1\right)(3h - 3h^2 + h^3) \\ \\ \quad + \left(\frac{1}{k_b} - 1\right)h^3 \end{array}\right\} \tag{3}$$

and:

$$\Delta\phi_{ba} = \Delta M_a . K_2 . L/EI \tag{4}$$

where:

$$K_2 = -\frac{1}{6}\left\{\left(\frac{1}{k_a} + \frac{1}{k_b} - 2\right)(3h^2 - 2h^3) + 1\right\} \tag{5}$$

Similarly when the moment at B changes by ΔM_b , it is found that:

$$\Delta\phi_{bb} = \Delta M_b . K_3 . L/EI \tag{6}$$

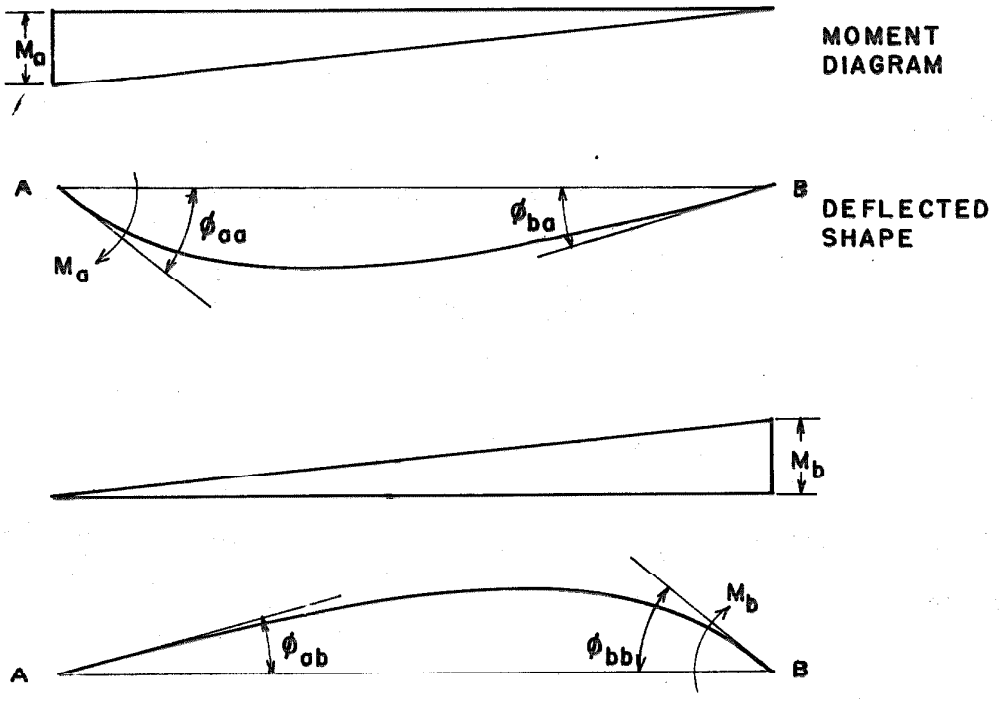

Figure 4a: Application of end moments to find member stiffness.

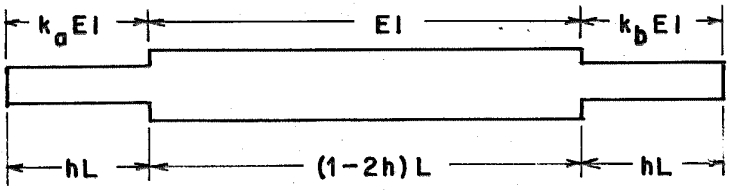

Figure 4b: Variation in flexural rigidity along a member.

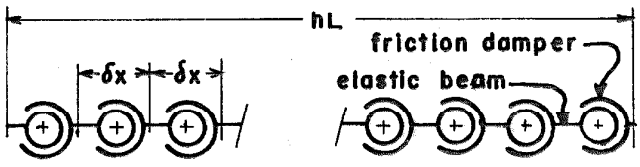

Figure 4c: Series connected beam-damper assembly.

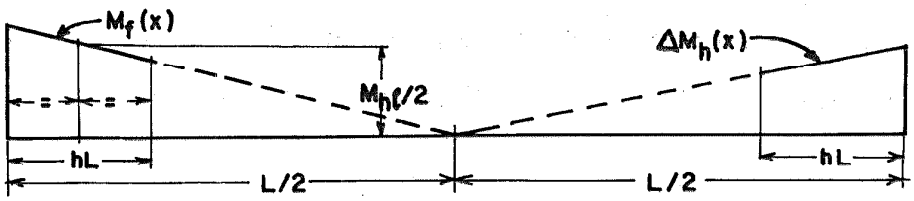

Figure 4d: Functions $M_f(x)$ and $\Delta M_h(x)$.

where:

$$K_3 = \frac{1}{3}\left\{ \begin{array}{l} 1 + \left(\frac{1}{k_b} - 1\right)(3h - 3h^2 + h^3) \\ \\ +\left(\frac{1}{k_a} - 1\right)h^3 \end{array} \right\} \tag{7}$$

and:

$$\Delta\phi_{ab} = \Delta M_b \cdot K_2 L/EI \tag{8}$$

When the changes ΔM_a and ΔM_b occur simultaneously, the corresponding changes in end rotation are:

$$\begin{aligned} \Delta\phi_a &= \Delta\phi_{aa} + \Delta\phi_{ab} \\ \Delta\phi_b &= \Delta\phi_{ba} + \Delta\phi_{bb} \end{aligned} \tag{9}$$

and hence from equations (2), (4), (6) and (8):

$$\begin{aligned} \Delta M_a &= \frac{EI}{L} \cdot \frac{(K_3\Delta\phi_a - K_2\Delta\phi_b)}{(K_1K_3 - K_2^2)} \\ \Delta M_b &= \frac{EI}{L} \cdot \frac{(-K_2\Delta\phi_a + K_1\Delta\phi_b)}{(K_1K_3 - K_2^2)} \end{aligned} \tag{10}$$

Because S_1, p, and p_r are defined only for the special loading case shown in figure 3a, k and k_r can be found by assuming:

$$\begin{aligned} \Delta M_a &= \Delta M_b = \Delta M_e \\ \Delta\phi_a &= \Delta\phi_b = \Delta\phi_e \\ k_a &= k_b \end{aligned} \tag{11}$$

Using these values in equations (3), (5), and (7), and substituting the values found for K_1, K_2, and K_3 into equation (10) gives:

$$\Delta M_e = \frac{6EI}{L} \cdot \left\{ \frac{1}{1 + (1/k_a - 1)(6h - 12h^2 + 8h^3)} \right\} \Delta \phi_e \qquad (12)$$

When $k_a = k_b = 1$ equation (12) gives:

$$\begin{aligned} \Delta M_e &= \frac{6EI}{L} \cdot \Delta \phi_e \\ &= S_1 . \Delta \phi_e \end{aligned} \qquad (13)$$

When $k_a = k_b = k$ the incremental $M_e - \phi_e$ equation is by definition:

$$\Delta M_e = pS_1 . \Delta \phi_e \qquad (14)$$

Thus from equations (12), (13) and (14)

$$p = \frac{1}{\{1 + (1/k - 1)(6h - 12h^2 + 8h^3)\}} \qquad (15)$$

Similarly:

$$p_r = \frac{1}{\{1 + (1/k_r - 1)(6h - 12h^2 + 8h^3)\}} \qquad (16)$$

Equations (15) and (16) are used to find values of k and k_r which give the required values of p and p_r for each value of h assumed.

In the response analysis each hinge length is considered independently, so that the overall stiffness of a member, which depends on the hinge conditions at each end, can differ from the stiffness when the member is loaded as shown in figure 3a. The incremental end moment-end rotation equation for a member is:

$$\begin{Bmatrix} \Delta M_a \\ \\ \Delta M_b \end{Bmatrix} = \frac{EI}{L} \begin{bmatrix} S_a & S_b \\ \\ S_b & S_c \end{bmatrix} \begin{Bmatrix} \Delta \phi_a \\ \\ \Delta \phi_b \end{Bmatrix} \qquad (17)$$

where S_a, S_b and S_c are found from equations (10) to be:

$$S_a = K_3/(K_1K_3 - K_2^2)$$

$$S_b = -K_2/(K_1K_3 - K_2^2) \qquad (18)$$

$$S_c = K_1/(K_1K_3 - K_2^2)$$

Since k_a and k_b can vary independently, and each can have the value 1, k, or k_r, nine stiffness matrices, each of which corresponds to a particular combination of hinge conditions, can be found for each member before the response analysis begins. During the analysis, the appropriate stiffness matrix for any member can then be found from a simple examination of the hinge conditions at each end.

The complex behavior of a real hinge, in which high concrete strains and bond slip both contribute to the reduction in stiffness and to the energy dissipation is represented here by the action of two beams acting in parallel, and joined along their length so that they always have identical deflected shapes. The first beam is always elastic, and cracking in the hinge length is assumed to reduce its flexural rigidity from EI to kEI. The second beam is shown in figure 4c. It is an assembly of series-connected elastic beams of infinitesimal length, separated by friction dampers which rotate whenever their friction moment is exceeded. The flexural rigidity of the series-connected beams is always such that whenever the dampers are not slipping, the combined flexural rigidity of the two parallel beams is k_rEI.

The behavior of the beam-damper assembly can be understood by considering what happens when equal end moments are applied to a member in the same sense to load it for the first time. Initially both of the parallel beams deflect elastically with a combined flexural rigidity of

$k_r EI$. When the moment at the mid-point of the beam-damper assembly reaches $M_{h\ell}/2$, all the friction dampers are assumed to start to slip, the effective flexural rigidity of the assembly falls to zero, and the flexural rigidity of the hinge falls to EI or kEI, according to whether θ_h is less than or greater than θ_c . If the bending moment at a distance x from the mid-point of the beam-damper assembly when slipping begins is given by the linear function $M_f(x)$, then the friction moment for each damper is assumed to be given by the same function $M_f(x)$, for as long as the slipping continues. When the first load reversal occurs, the dampers stop slipping, and the assembly again behaves like an elastic beam. The hinge length has stiffness $k_r EI$, and the moment carried by the beam-damper assembly starts to fall. When it reaches $-M_{h\ell}/2$ at the mid-point, all the dampers again begin to slip, with some new linear variation of the friction moment along the assembly. Thus the beam-damper assembly controls the energy dissipation and the reversal stiffness of the hinge length.

The energy dissipated by one hinge length, ΔD_h , when the dampers are slipping and the hinge moment changes by ΔM_h . is found by summing the energy dissipated by the individual dampers. If the linear function giving the value of ΔM_h at some distance x from the mid-point of the hinge is $\Delta M_h(x)$, then:

$$\Delta D_h = \int_{-hL/2}^{hL/2} M_f(x) . \Delta M_h(x) . \frac{dx}{FR_h} \qquad (19)$$

When calculating ΔD_h it was assumed that $M_f(x)$ and $\Delta M_h(x)$ were always functions like those shown in figure 4d, which is equivalent to

assuming that for every member the end moments are equal and in the same sense throughout the analysis, so that $\Delta M_h(x)$ and $M_f(x)$ can then be written:

$$\Delta M_h(x) = \Delta M_h\{1 + 2x/(1 - h)L\}$$
$$M_f(x) = M_{h\ell}\{1 + 2x/(1 - h)L\}/2 \qquad (20)$$

If h is taken as 0.2, (the value used for all the prestressed members), equations (19) and (20) give:

$$\Delta D_h = 1.021.\frac{hL}{FR_h}\Delta M_h.\frac{M_{h\ell}}{2} \qquad (21)$$

Although both $\Delta M_h(x)$ and $M_f(x)$ vary from the assumed distribution, the end moments acting on a member are usually approximately equal and opposite, and the assumed distributions are adequate for finding the hysteretic energy dissipated by the structure.

The width, $M_{h\ell}$, of the $M_h - \theta_h$ loop is chosen so that the $M_e - \phi_e$ loop has the specified width $\ell.M_c$ when the member is loaded by the application of equal end moments acting in the same sense, and the hinge lengths are cracked when the reversal occurs. For this case it follows from the definition of M_h that the change in end moment, M_r, when the $M_e - \phi_e$ loop is crossed during the reversal, is related to the change in hinge moment, M_{hr}, when the $M_h - \theta_h$ loop is crossed, by:

$$M_r = M_{hr}/(1 - h)$$

Consideration of the gradients of the loading and reversal paths (see figures 1 and 3c) shows that the width of the $M_e - \phi_e$ loop is:

$$M_\ell = \ell.M_c = M_r(1 - p/p_r) \qquad (23)$$

Similarly, for the $M_h - \theta_h$ loop:

$$M_{h\ell} = M_{hr}(1 - k/k_r) \tag{24}$$

From equations (22), (23) and (24) it can be seen that:

$$M_{h\ell} = \ell . M_c (1 - h) \frac{p_r . (k_r - k)}{k_r (p_r - p)} \tag{25}$$

and this equation is used to find $M_{h\ell}$. The width of $M_h - \theta_h$ loop is kept constant, but the actual width of an $M_e - \phi_e$ loop during the analysis will only be $\ell . M_c$ if the most recent reversal occurred simultaneously at both ends of the member, and both hinges were cracked at the time it occurred. If both hinges are uncracked, and a reversal occurs simultaneously at both ends, the width of the $M_e - \phi_e$ loop will be less than $\ell . M_c$, and is given by:

$$M_\ell = \ell . M_c \frac{(p_r - 1)(k_r - k)}{(p_r - p)(k_r - 1)} \tag{26}$$

Thus both the slope and the width of each $M_e - \phi_e$ loop vary during the analysis, and the $M_e - \phi_e$ loops are not always the same at both ends of a member.

To model the $M_e - \phi_e$ loop for the reinforced concrete member, shown in figure 2, the reversal stiffness factor k_r is taken as 1, and the loopwidth, M_ℓ, of the $M_e - \phi_e$ loop is:

$$M_\ell = 2 . M_c (1 - p) \tag{27}$$

The criterion for cracking, (or yielding), is based on the hinge moment, M_h, rather than the hinge rotation, θ_c.

In the response analysis, the initial loading of a prestressed member is assumed to be along the backbone curve of the $M_e - \phi_e$ loop, and not along a reversal path as discussed above.

4. VISCOUS DAMPING

Because complete information is not available about the damping mechanisms in real structures, two viscous damping mechanisms commonly used in structural analysis are assumed, in addition to the hysteretic damping in the members. The first, mass proportional viscous damping, is expressed by:

$$\alpha M \dot{\underline{U}}$$

where α is a scalar constant, M is the 20 x 20 diagonal mass matrix, and $\dot{\underline{U}}$ is the vector of velocities of the floors relative to the ground. The second mechanism is a form of interfloor viscous damping, expressed by:

$$\beta K \dot{\underline{U}}$$

where β is a scalar constant and K is the tri-diagonal stiffness matrix for the special case when all girders are assumed to be rigid, and the columns are flexible but do not crack. These expressions appear in the linear matrix equation of motion as:

$$M\ddot{\underline{y}} + (\alpha M + \beta K)\dot{\underline{U}} + K'\underline{U} = 0 \qquad (28)$$

where $\ddot{\underline{y}}$ is the vector of absolute story accelerations, K' is the 20 x 20 full stiffness matrix for the real structure with flexible columns and girders, and $\underline{U}$ is the vector of story displacements relative to the ground.

For mass proportional damping only, the fraction of critical damping in the first mode, ξ_m, is given by:

$$\xi_m = \frac{\alpha}{2\omega_1} \tag{29}$$

where ω_1 is the circular natural frequency of the first mode. For true stiffness proportional interfloor viscous damping only, expressed by:

$$\beta' K' \dot{\underline{U}}$$

where β' is a scalar constant, the fraction of critical damping in the first mode is:

$$\xi_i' = \frac{\beta' \omega_1}{2} \tag{30}$$

To find an equivalent fraction of critical damping, ξ_i, for the nonproportional interfloor damping mechanism actually used, the two mechanisms $\beta K \dot{\underline{U}}$ and $\beta' K' \dot{\underline{U}}$ are assumed to be equivalent if both dissipate the same amount of energy per cycle, when the structure is vibrating with frequency ω_1 and displacement vector $\underline{U}_1 \sin(\omega_1 t)$, where $\underline{U}_1$ is the first mode shape for the undamped structure. This requires that:

$$\beta U_1^t K U_1 = \beta' U_1^t K' U_1 \tag{31}$$

For the structure analyzed equation (31) gives:

$$\beta' \approx 3.3\beta \tag{32}$$

Using equation (30), ξ_i is found to be:

$$\xi_i = \frac{3.3\beta\omega_1}{2} \tag{33}$$

The choice of an interfloor damping mechanism using K rather than K' was made to reduce computational difficulties.

5. NONLINEAR EQUATIONS OF MOTION

The nonlinear equations of motion were solved with a computer, using a step-by-step integration technique with finite time increments. The structure was assumed to remain linear throughout any given time increment, so the nonlinear response is the sum of the results of a series of incremental linear analyses. A matrix substitution method (4), (5), was used to solve the linear equations of motion for each time increment, and member properties were varied if necessary before the next increment began. The foundation of the structure was assumed to be rigid, and torsion was neglected. The masses were concentrated at the floor levels and only moved horizontally, and the floors contributed no additional stiffness.

The magnitude of the time increment used was 0.005 seconds, which is approximately one sixth of the period of the 20^{th} mode.

The hysteretic energy, ΔD_h, dissipated by each hinge was found after every incremental analysis. The incremental viscous energy dissipation at each floor level was found by assuming that a force, equal to the mean of the viscous forces acting at the beginning and end of the increment, acted throughout the interval. Mass proportional and inter-floor viscous energy dissipations were found separately.

6. EXCITATION

The excitation used in each analysis was the first 8 seconds of the accelerogram of the El Centro 1940 earthquake, N-S component. This has a peak acceleration of 0.32g, which occurs 2 seconds after the start of the record, and a peak spectral frequency of 14 rad/sec (6).

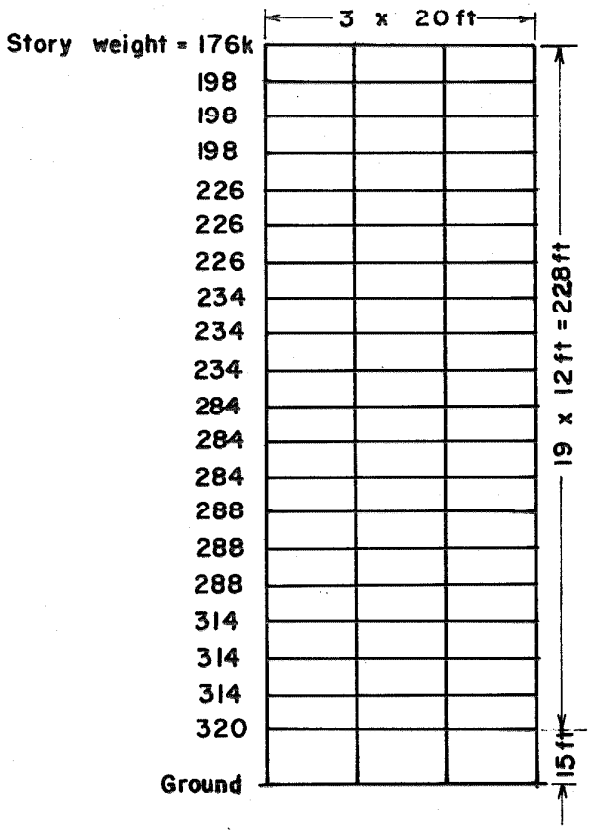

Figure 5: Properties of structure

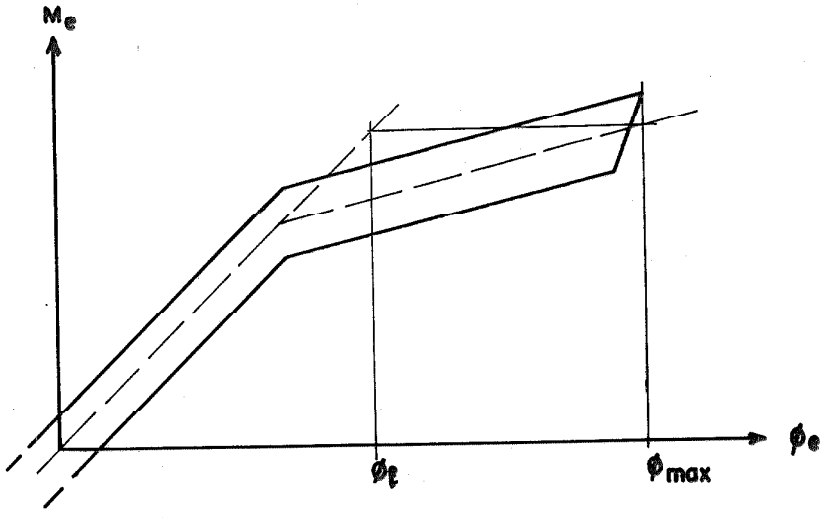

Figure 6: Definition of ϕ_{max} and ϕ_{ℓ} for member ductility factor.

7. STRUCTURE ANALYZED

The properties of the basic structure analyzed are shown in figure 5 and Table 1. It was designed by Clough and Benuska (7), who found the relative stiffnesses of the members by applying dead loads and live loads plus code (8) lateral forces for earthquake. Member flexural rigidities were specified in terms of a reference value, $EI_o = 133,500$ Kip. ft.^{2} which gave a natural period of 2.2 seconds. An exact computer analysis was then made to find the "design" moments resulting from the static application of the horizontal and vertical design forces. Cracking moments were taken as twice the design moments for the girders, and six times the design moments for the columns. Two reinforced and five prestressed concrete versions of this structure are considered here. A sixth prestressed concrete structure had both column and girder cracking moments equal to twice their design moments.

8. RESULTS PRESENTED

All the results discussed, except those for dissipated energy, are maximum values recorded during the eight seconds of earthquake excitation.

As a measure of nonlinear deformation, two different ductility factors were found for each end of every member. The member ductility factor, μ_m, is:

$$\mu_m = \begin{cases} \dfrac{\phi_{max}}{\phi_\ell} & (\phi_{max} \geq \phi_c) \\ \dfrac{\phi_{max}}{\phi_c} & (\phi_{max} < \phi_c) \end{cases} \tag{34}$$

where ϕ_{max} is the maximum recorded end rotation, and ϕ_{ℓ} is found as shown in figure 6. using the $M_e - \phi_e$ loop for equal end moments applied to the member as shown in figure 3a.

The hinge ductility factor, μ_h, is:

$$\mu_h = \frac{\theta_{max}}{\theta_c} \tag{35}$$

where θ_{max} is the maximum recorded hinge rotation. With the beam model used, μ_m is generally less than μ_h, because the member stiffness reduction factor, p, is greater than the hinge stiffness reduction factor, k. Ductility requirements for structural members are usually given in terms of member ductility factors similar to μ_m, but some test results (1) have been given in terms of hinge ductility factors.

Values of the base overturning moment, M_b, and the compressive force at the base of the exterior column, F_c, result from the moments and shears induced by lateral displacement of the structure, and do not include gravity and dead load effects.

The results given for dissipated energy are all based on cumulative totals for the eight seconds of excitations. Values for the entire structure are: The total energy dissipated, D_t; the ratio of viscous to hysteretic energy dissipation, D_v/D_h; and the ratio of mass proportional to interfloor viscous energy dissipation, D_{vm}/D_{vi}. Some values of the energy dissipated on each story level are given graphically.

In addition, plots of the variation of certain response parameters during the 8 secs of excitation are given in Appendix A.

9. DISCUSSION OF RESULTS

Reinforced Concrete Structures: For comparison with the prestressed structures, two structures with members having $M_e - \phi_e$ properties as shown in figure 2 were analyzed. Both had $p = 0.05$ for all members. The hinge length factors were $h = 0.05$ for the girders, and $h = 0.07$ for the columns, giving hinge lengths of 12 in. and 10 in. respectively, which are similar to observed values (1). Structure 1 had mass proportional viscous damping only, with $\xi_m = 0.1$. Structure 2 had interfloor viscous damping only, with $\xi_i = 0.05$. Nonlinear response results for structure 1 have been found previously (5), (7). It is assumed here that these structures, with their elasto-plastic members, could satisfactorily withstand a strong earthquake.

Figure 7 shows that the mass proportional damping is more effective in controlling lateral displacements, but figures 9, 11 and 13 show that the interfloor damping is more effective in controlling interstory drift, girder member ductility, and girder hinge ductility respectively. Table 2 confirms this for the maximum column ductility factors. The interfloor damping controls nonlinear deformations more effectively because it has a progressively greater effect on the higher modes. Figures 11 and 13 also show the significant difference between the largest values of μ_m (4.3) and μ_h (16.8) for the girders of structure 1. Although the beam model used is a simple one, a similar difference between μ_m and μ_h might be found for real members.

Table 2 shows the effectiveness of the specified interfloor damping in reducing the maximum absolute story acceleration, A. The value of 0.82g for structure 1, recorded on the 17^{th} floor, is probably high

enough to damage non-structural elements and equipment. The value of 0.31g for structure 2, recorded on the first floor, is less than the maximum base acceleration of 0.32g and seems too low to be realistic.

The significance of the values of M_b and F_c given in Table 2 is discussed later.

Figures 14 and 15 show how much energy was dissipated at each floor level by viscous damping and by hysteretic damping, for structures 1 and 2 respectively. Table 2 gives energy dissipation results for the entire structures. It seems clear from these results that neither of the viscous damping mechanisms used accurately model mechanisms likely to operate in real structures. The gradual fall in energy dissipation toward the base with mass proportional damping, and the sharp peaks for certain floors with interfloor damping, both appear to be rather unrealistic. However, the use of these mechanisms when comparing the responses of different structures appears to be justified, until more accurate models of the real mechanisms are available. Because of the simple $M_e - \phi_e$ diagram used, there is no hysteretic energy dissipation when elastic hinge rotation occurs after some plastic rotation has been incurred by a hinge, so that the relatively large values of D_v/D_h (0.70 and 1.15) are perhaps not unreasonable.

Prestressed Concrete Structures: The basic prestressed structure had the same member flexural rigidities and cracking moments as structures 1 and 2. This is not intended to represent an economical prestressed design — it is used to show the effects of a direct substitution of prestressed for reinforced concrete members. The hinge length factor used for all members, $h = 0.2$, was based on exprerimentally observed values (2).

The reversal stiffness factor was $p_r = 2.0$, to ensure that the $M_e - \phi_e$ loops were crossed reasonably quickly.

In structure 3 the stiffness reduction and loopwidth factors used were $p = 0.2$ and $\ell = 0.2$ for the girders, and $p = 0.5$ and $\ell = 0.5$ for the columns. These values are based on test results (2). The girder and column values are different because the columns have a higher ratio of cracking to design moment than the girders. This requires a higher prestress in the columns, which increases p and tends to reduce ℓ (by reducing cracking and bond slip). It also results in less post-cracking deformation, which further increases p and reduces ℓ. Mass proportional viscous damping, with $\xi_m = 0.1$, was used.

The lateral story displacements shown in figure 7 are all larger than the corresponding values for structure 1, which had similar viscous damping. The interstory drifts shown in figure 9 are also generally greater than those of structure 1, although the maximum drift recorded for structure 3 (1.1 in.) is less than that for structure 1 (1.29 in.). Values of μ_m for the girders, shown in figure 11, have a maximum of 2.6, and Table 2 shows the maximum column value is only 1.7. These values show that although the interfloor deflections might be large enough to cause non-structural damage, no structural damage to the members should occur, since member ductility factors of at least four are possible, without structural damage, for properly designed prestressed members.

Figure 13 shows that the maximum value of μ_h for the girders is 5.4, compared with 16.8 for structure 1. This difference is partly due to the greater hinge length assumed for the prestressed members. The simple beam model used gives no indication of how the curvature is distributed within the hinge length, but prestressing does delay the

development of curvature concentrations due to steel yielding, so these values of μ_h should give an indication of the relative amounts of concrete distress to be expected within prestressed and reinforced concrete hinges.

Table 2 shows that the maximum story acceleration, A , is only slightly higher than for structure 1, but the values of M_b and F_c are much higher. These are discussed later.

The ratio $D_v/D_f = 2.28$ in Table 2 is higher than that for structure 1, and suggests that too much viscous damping has been included.

In structure 4, the viscous damping was changed to interfloor damping, with $\xi_i = 0.05$. The other parameters were the same as for structure 3. The lateral displacements shown in figure 7 are all larger than those for structure 3 and the interstory drifts shown in figure 9 are generally larger. Figure 11 and Table 2 show ductility factors which reflect these changes. The values of A in Table 2 show that interfloor damping reduced the absolute story accelerations, just as it did for structure 2.

The ratio of $D_v/D_f = 2.82$ was higher than that for structure 3, although the viscous damping factor was less. This value suggests that as in structure 3, viscous damping is responsible for too much of the total energy dissipation. The sharply peaked curve for D_v in figure 16 suggests that this is in part the result of the high relative interstory velocities associated with the higher modes. This confirms that until more information is available about damping mechanisms, these results should only be used for comparative purposes.

In structure 5, both types of viscous damping were included, with $\xi_m = 0.01$ and $\xi_i = 0.02$. Figures 8 and 10 show that the lateral displacements and the interstory drifts all exceeded those of structures 3 and 4. Ductility factors were also correspondingly large, but as seen from figure 12 and Table 2, did not indicate excessively large nonlinear member deformations.

Table 2 shows that the base overturning moment, $M_b = 98 \times 10^3$ Kip. ft., and the external column compressive force, $F_c = 1376$ Kips., were also the highest recorded. The dead load contribution to M_b found by simultaneously giving each story its maximum lateral displacement was only 4.3×10^3 Kip. ft., or about 5% of M_b, so from this point of view the lateral displacements are apparently not excessive. Since the static moment required for overturning is 154×10^3 Kip. ft., it is the axial column load at the base which is more significant.

For each structure the static dead load produces a compressive force in the outer columns of 860 Kips. The application of the code (9) lateral loads for earthquake, (with no reduction factor for overturning moment) adds only another 335 Kips., whereas Table 2 shows that F_c, the maximum value of the added compressive force due to dynamic loading, varied from 847 Kip. for structure 1 to 1376 Kips. for structure 5. Thus static design methods give a very low estimate of column compressive forces.

The dissipated energy values in Table 2 show that reducing the amount of viscous damping has only reduced D_v/D_h to 1.91. The ratio of $D_{vm}/D_{vi} = 0.22$ shows the much greater effectiveness of the inter-floor damping in dissipating energy.

For structure 6 it was assumed that some of the energy dissipated by walls, floors, partitions, etc., could be included in the $M_e - \phi_e$ loops. Loopwidth factors were doubled, giving $\ell = 0.4$ for the girders and $\ell = 0.1$ for the columns. Viscous damping was the same as for structure 5, with $\xi_m = 0.01$ and $\xi_i = 0.02$. Figures 8, 10 and 12 and Table 2 show that the increased hysteretic damping was effective in reducing the response. The ratio $D_v/D_h = 0.91$, and a total energy dissipation, D_t, only slightly higher than for structure 5, suggest that as more hysteretic energy dissipation is assumed, the viscous damping becomes more acceptable.

In structure 7, the stiffness reduction factors were halved, giving $p = 0.1$ for the girders and $p = 0.25$ for the columns. Viscous damping and loopwidths were the same as for structure 6, and the results given in figures 8, 10 and 12, and in Table 2, should be compared with the results for that structure. A small increase in displacements and deformations, and a decrease in M_b and F_c, can be seen, so that changing p does not appear to significantly affect the response.

Structure 8 represents a more practical prestressed design, in which column cracking moments were reduced to only twice the design moments. This would allow a prestress of about 1000 psi in typical members, assuming an elastic modulus for concrete of 3×10^6 psi for this type of loading (2). Factors of $p = 0.2$, (suggested by test results (2)) and $\ell = 0.4$ (as for structure 6), were used for all members. Viscous damping was included, with $\xi_m = 0.01$ and $\xi_i = 0.02$. Figure 17 shows the energy dissipated on each floor. The reduction in the peak values of the interfloor viscous energy dissipation compared with

structures 2 and 4 is very marked, and the combination of viscous and hysteretic damping used in structure 8 appears to be reasonable. A comparison of the results in figures 8, 10, 12 and 17, and in Table 2, with those for the other structures, including the two reinforced structures, suggests that if allowance is made for relatively high interstory drifts and compressive forces in the columns, structure 8 would represent a satisfactory design to withstand the earthquake excitation used.

10. CONCLUSIONS AND SUMMARY

From this comparative study it appears that a prestressed concrete structure similar to that analyzed could be designed to withstand a strong earthquake. There would apparently be no structural damage to the prestressed concrete members, but non-structural damage as a result of excessive interstory drift might be more widespread than with a reinforced concrete frame. Large compressive forces in the exterior columns would have to be allowed for.

Efforts to control response by increasing hysteretic energy dissipation would be well worthwhile, but there seems little to be gained by increasing p.

The damping mechanisms which operate in structures, and which in reality depend on the performance of all the elements in the structure, both structural and nonstructural, are not yet well enough understood to permit an exact quantitative analysis of earthquake response. Further, such factors as ground-structure interaction, coupling between translational and torsional modes, and changes in structural properties resulting from the earthquake excitation, cannot be neglected if exact, quantitative

results are sought. But a comparative study like that made here, involving some structures which can be assumed to be satisfactory for earthquake loading, is a valuable way of using existing knowledge and analytical techniques to investigate the behaviour of new types of structure.

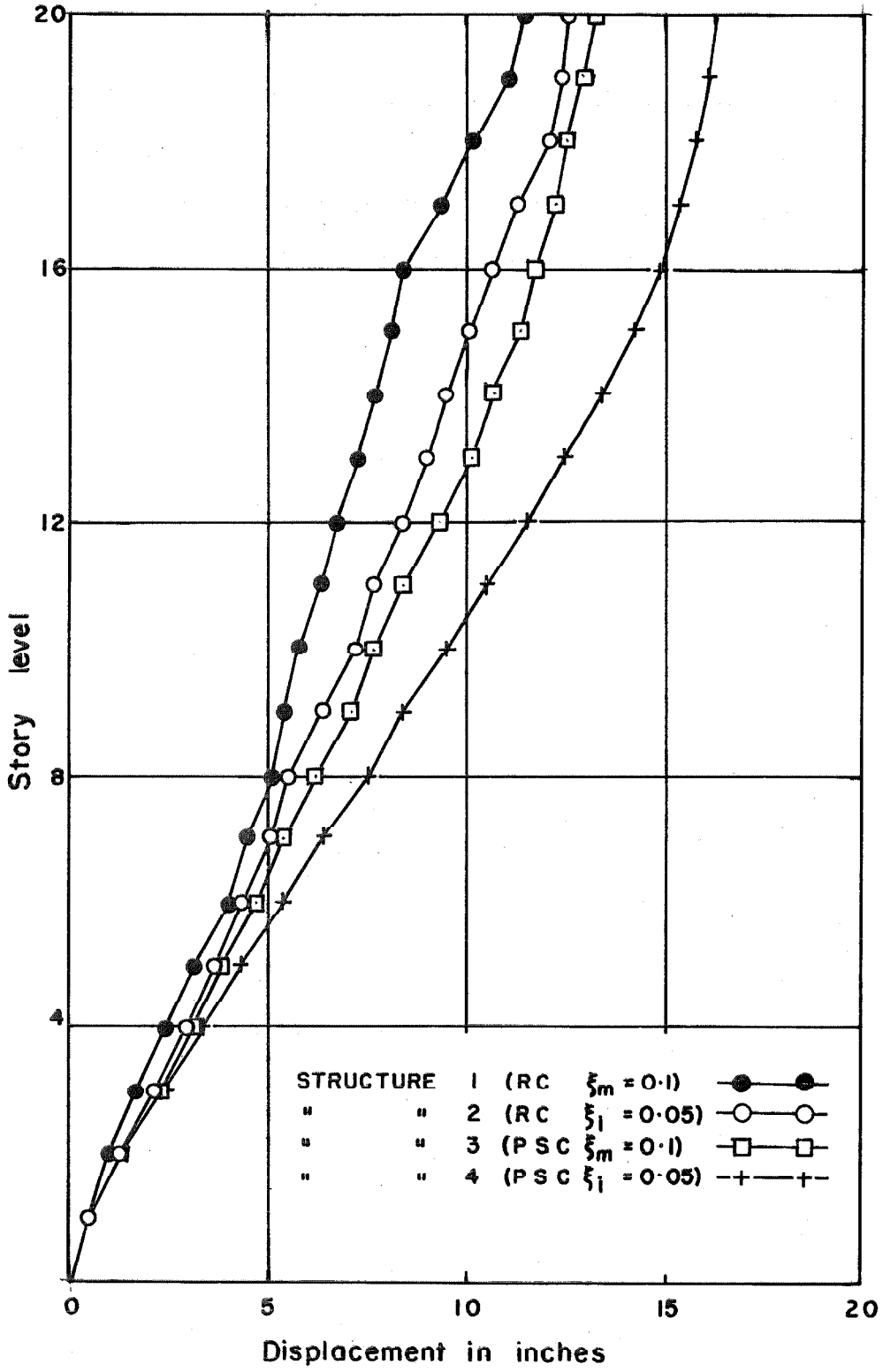

Figure 7: Maximum story displacements relative to the ground.

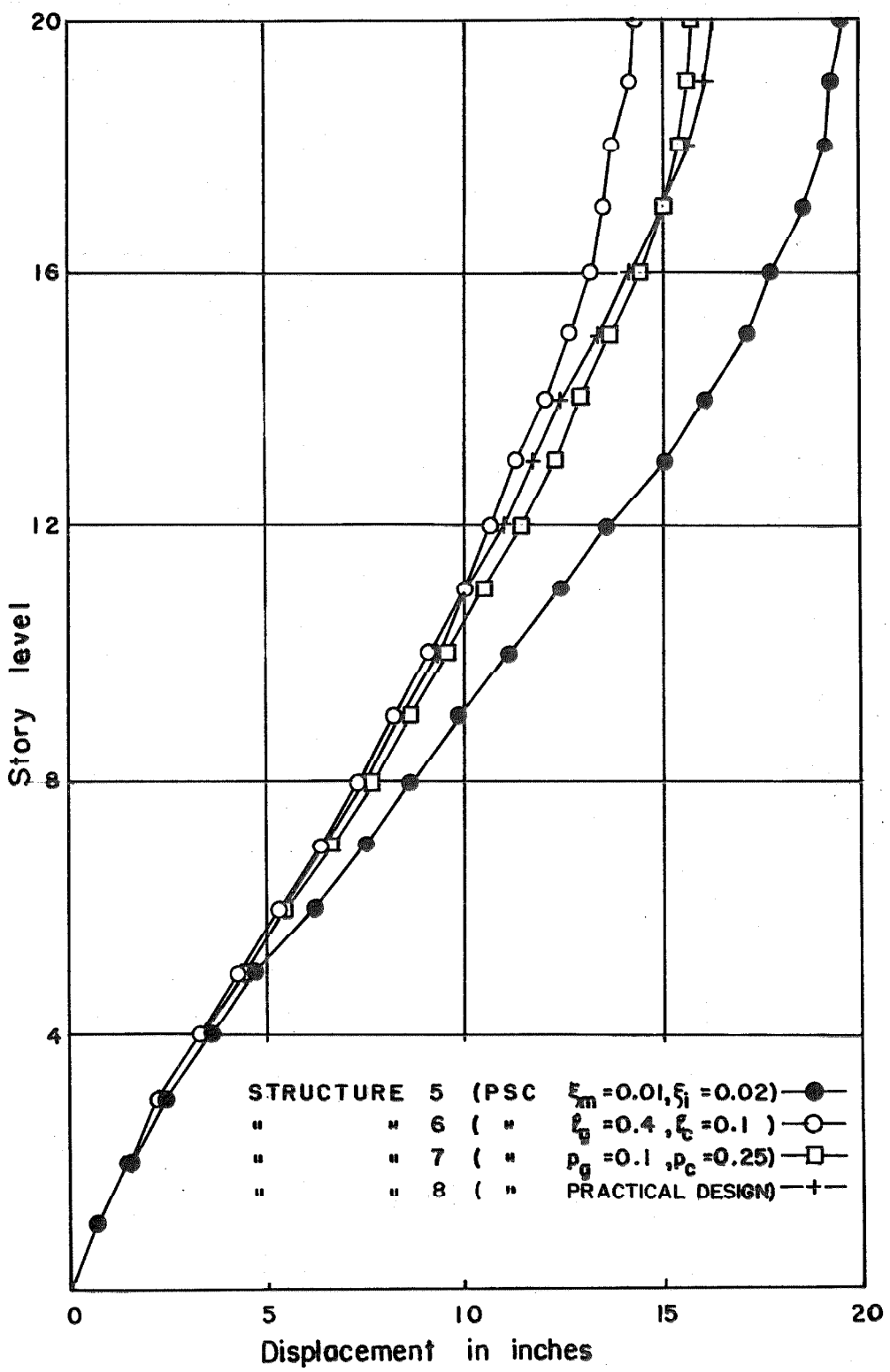

Figure 8: Maximum story displacements relative to the ground.

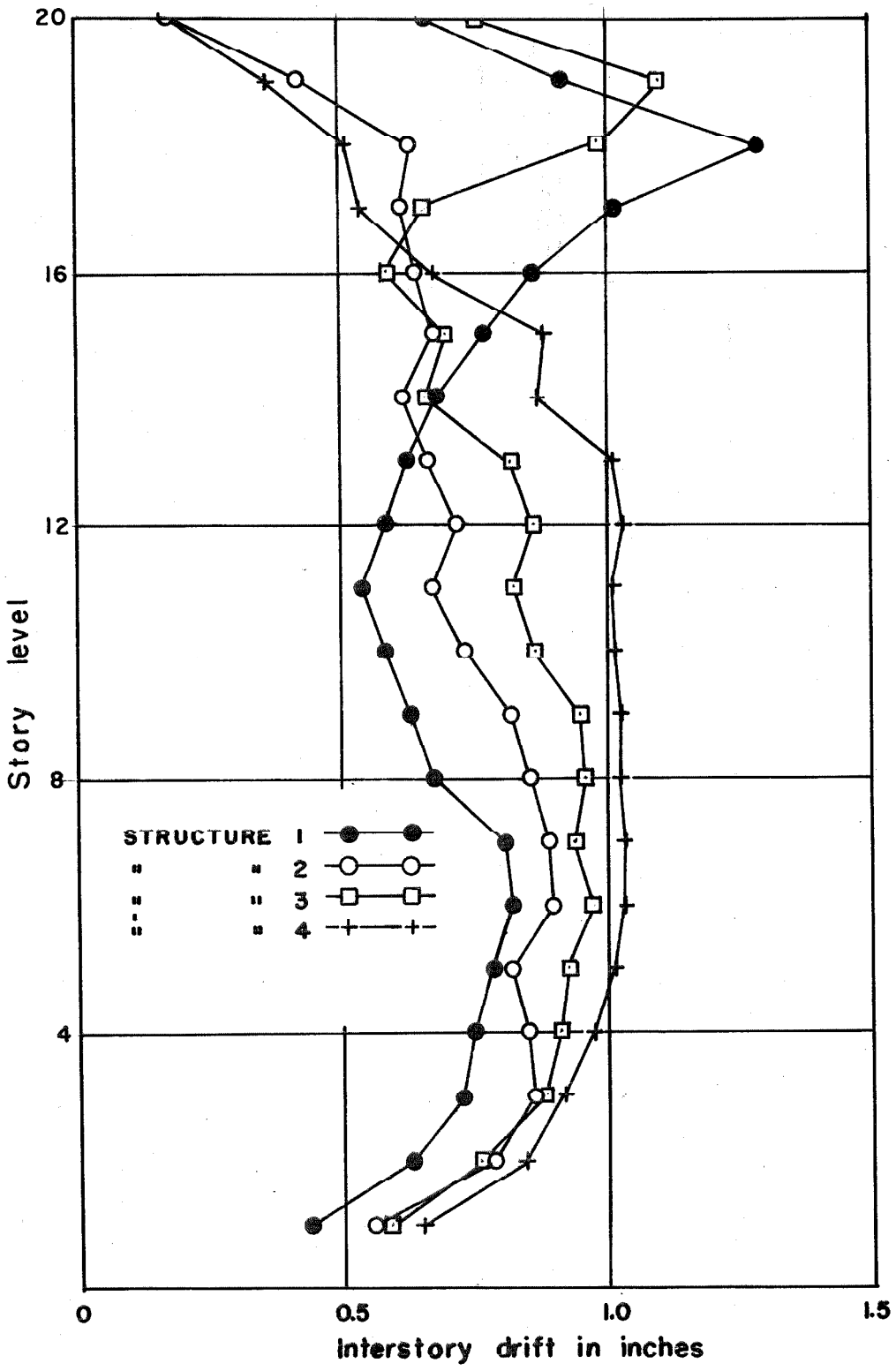

Figure 9: Maximum interstory drifts.

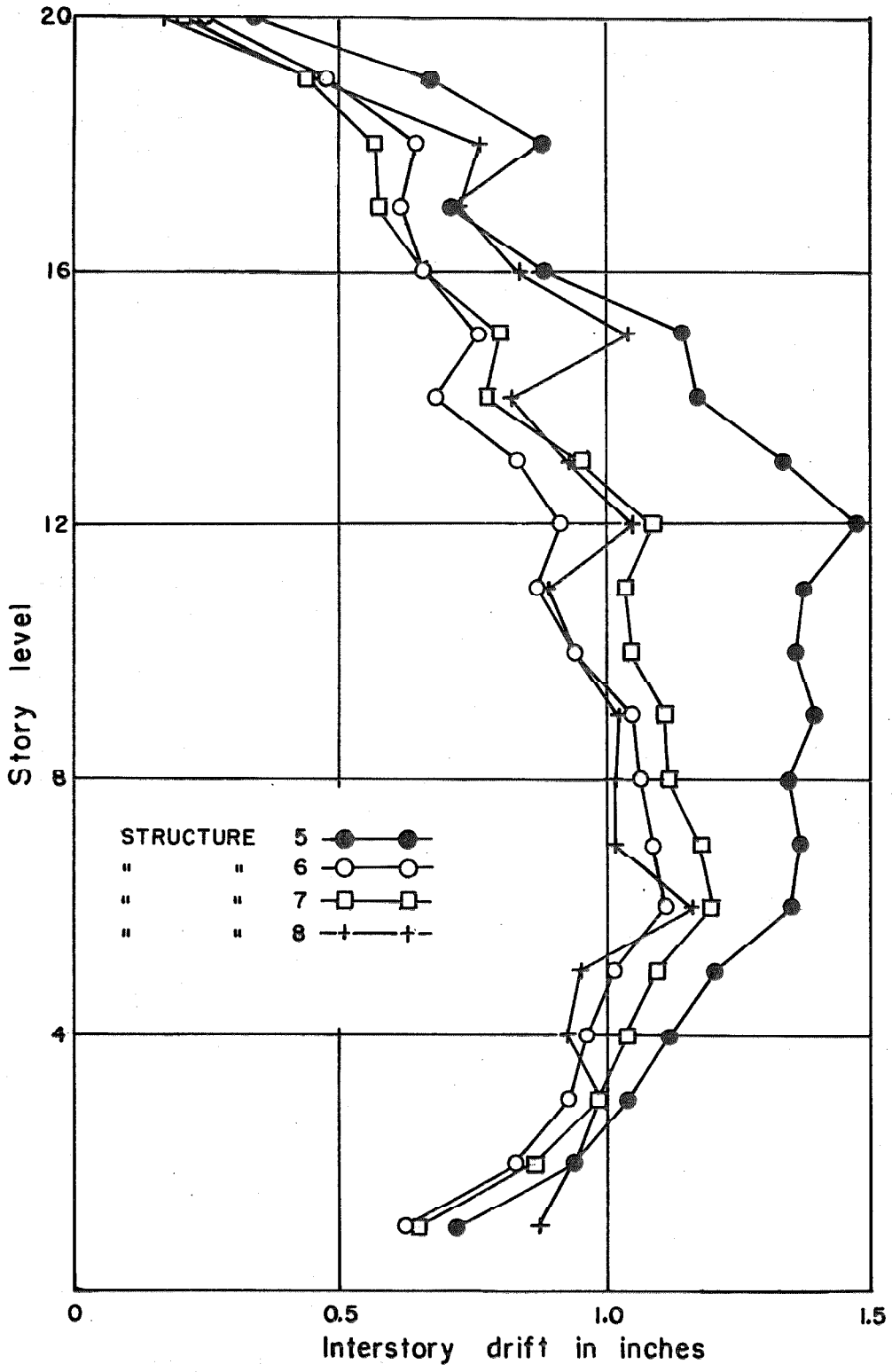

Figure 10: Maximum interstory drifts.

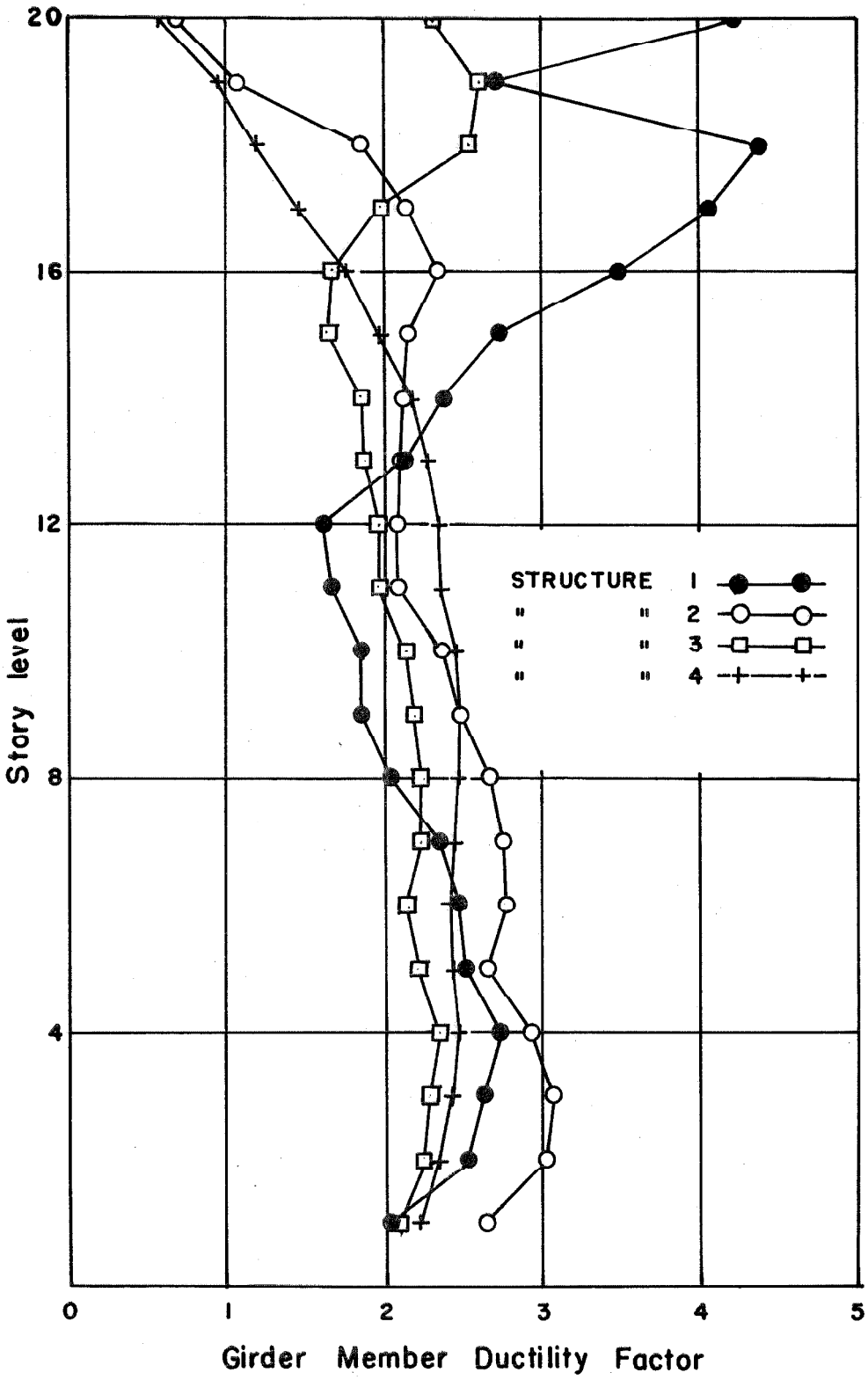

Figure 11: Maximum member ductility factors for the girders

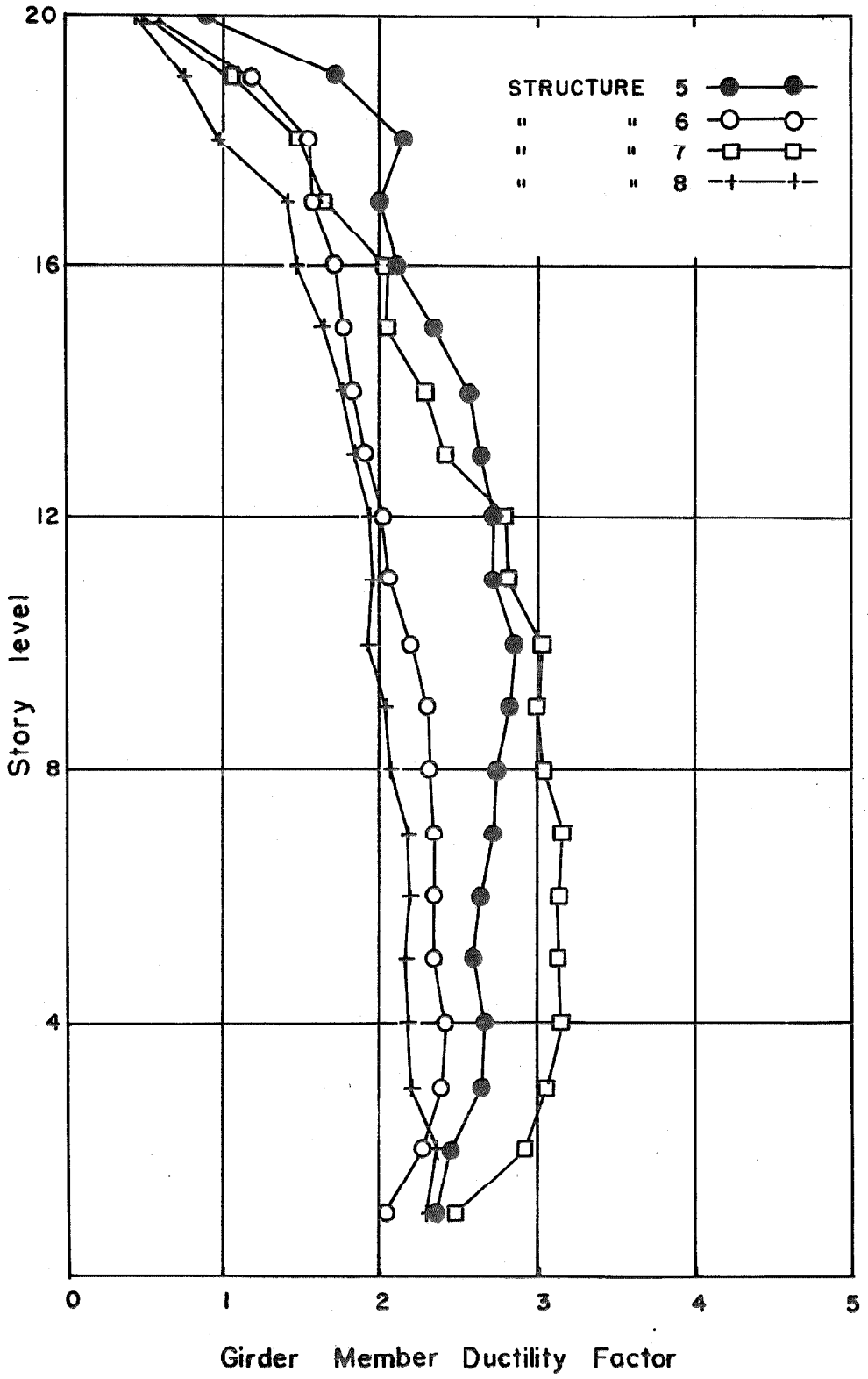

Figure 12: Maximum member ductility factor for the girders.

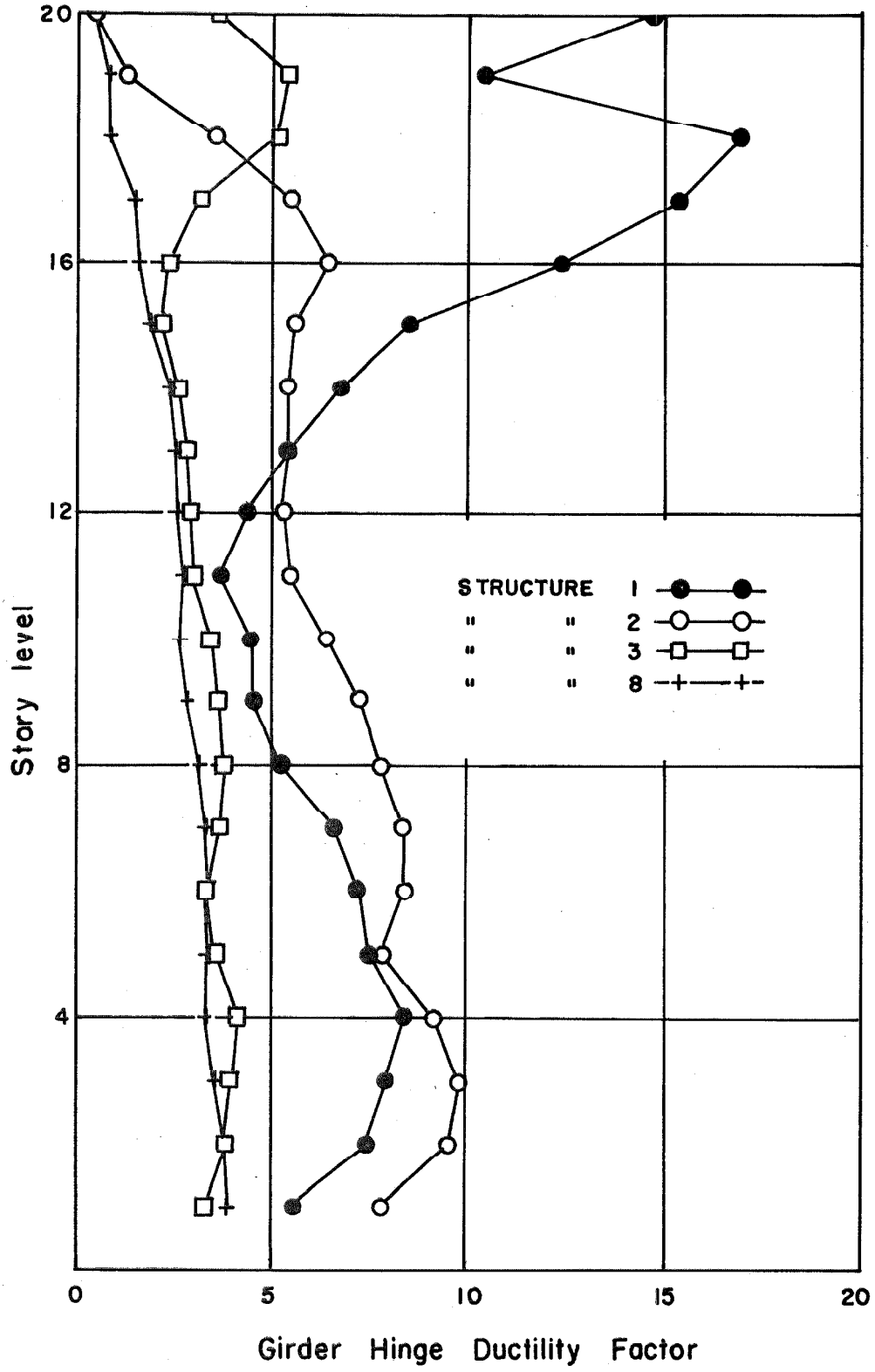

Figure 13: Maximum hinge ductility factors for the girders

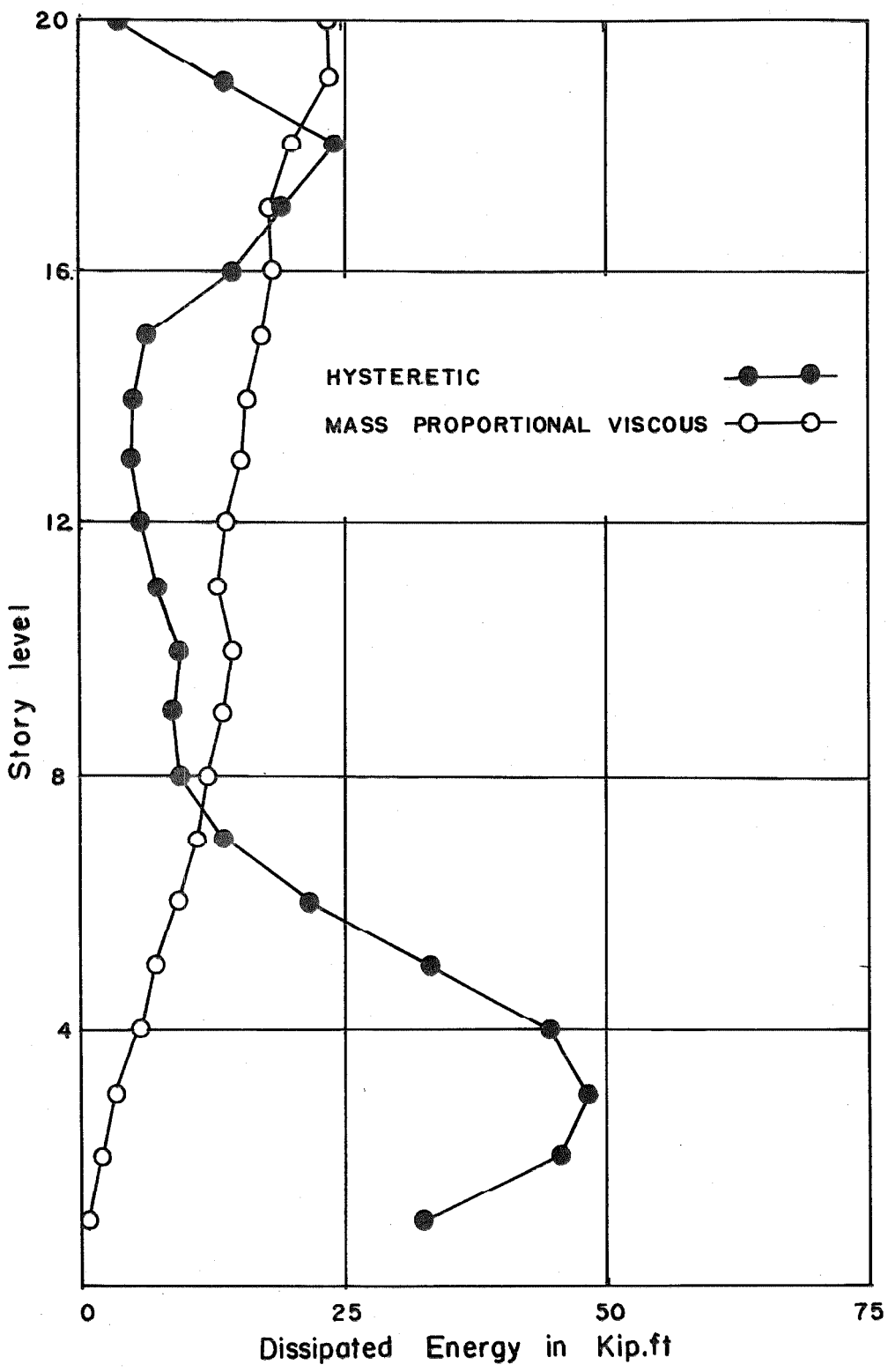

Figure 14: Structure 1: Energy dissipated at each story.

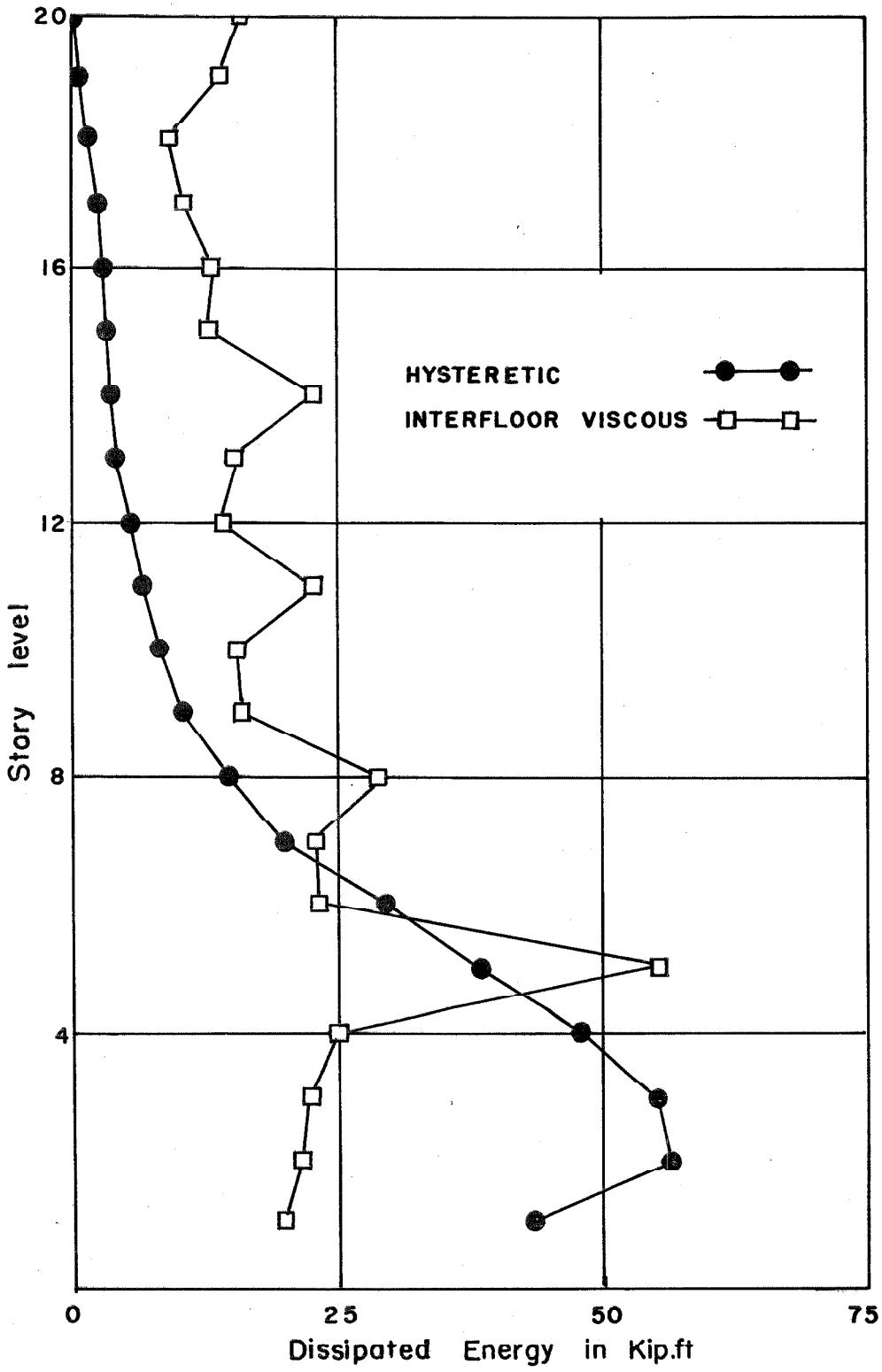

Figure 15: Structure 2: Energy dissipated at each story.

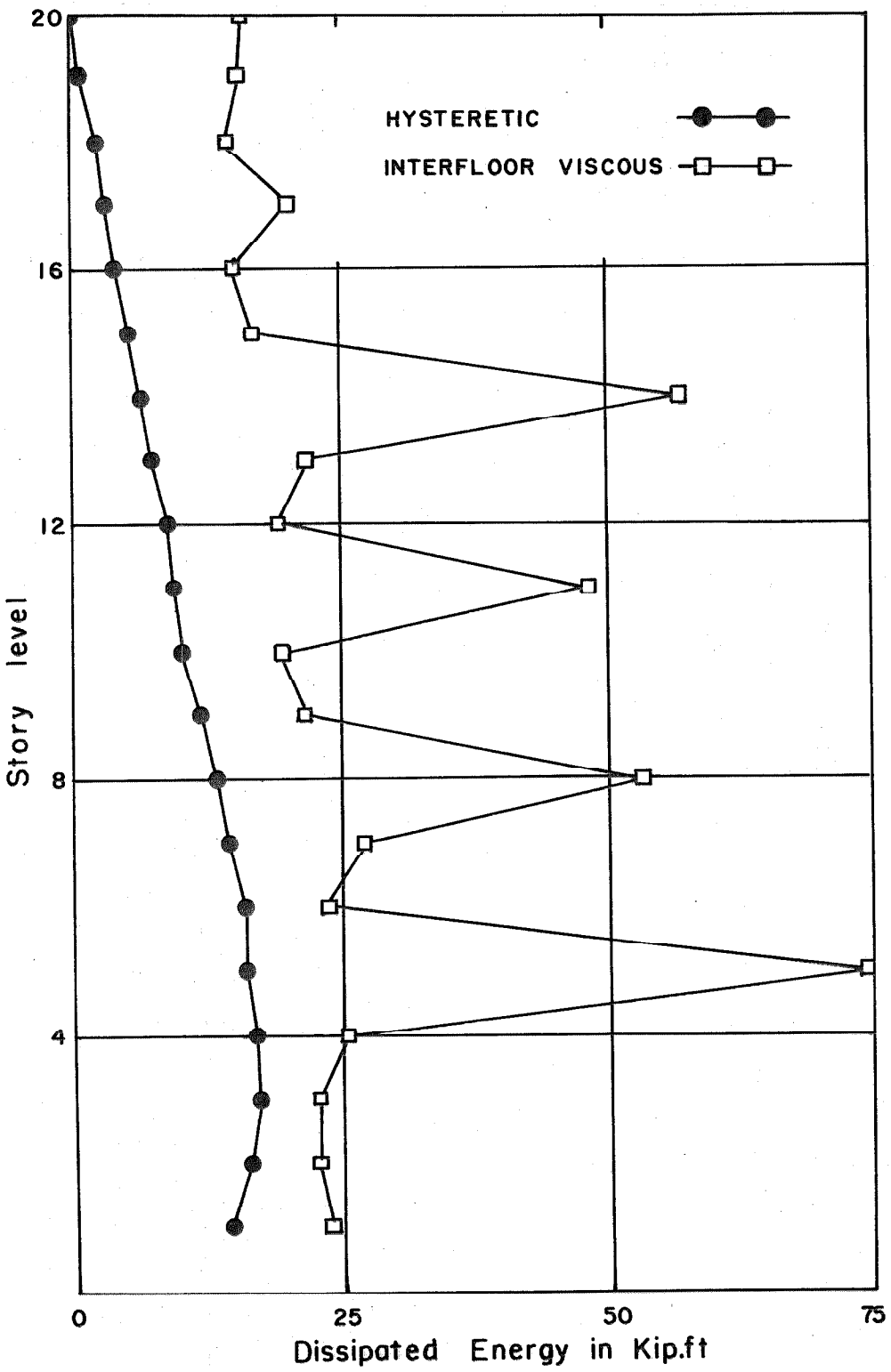

Figure 16: Structure 4: Energy dissipated at each story.

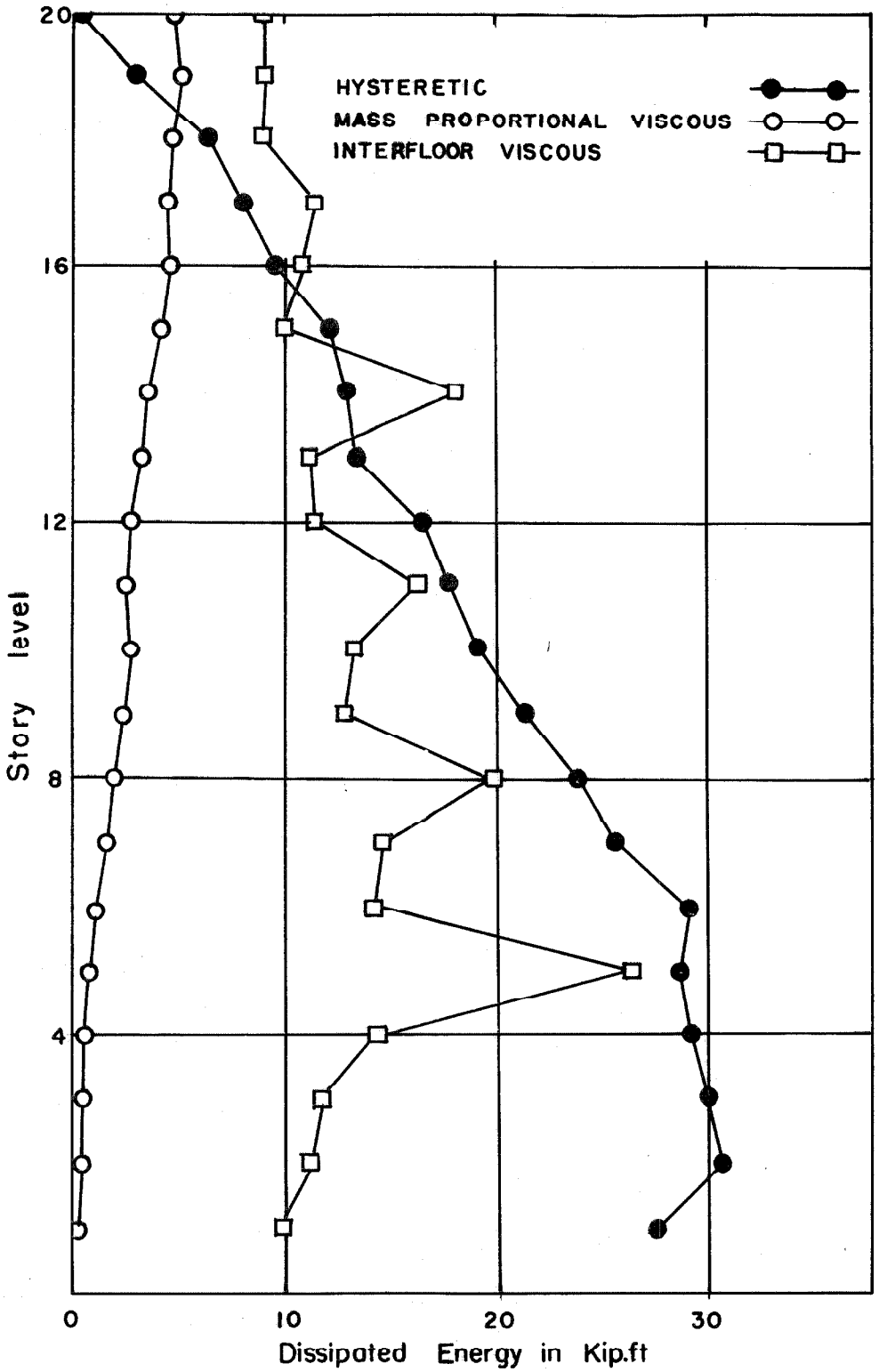

Figure 17: Structure 8: Energy dissipated at each story.

TABLE 1: RELATIVE FLEXURAL RIGIDITIES OF STRUCTURAL MEMBERS

Story Levels	EI/EI_o		
	Columns		Girders
	Exterior	Interior	
20-18	1.0	2.0	4.0
17-15	1.5	3.0	6.0
14-12	3.0	6.0	8.0
11-9	4.5	9.0	
8-6	6.0	12.0	
5-3	10.0	20.0	10.0
2-1	12.0	24.0	

TABLE 2: MAXIMUM VALUES OF RESPONSE PARAMETERS

Structure	Col. Ductility		A	M_b	F_c	D_{vm}/D_{vi}	D_v/D_h	D_t
	Member	Hinge	(frac. of g)	(Kip. ft. x 10^3)	(Kips.)			(Kip. ft.)
1	2.9 (20)[I]	7.2 (20)[I]	0.82 (17)[I]	55	847	—	0.70	626
2	0.8 (1)	0.8 (1)	0.31 (1)	59	916	—	1.15	752
3	1.7 (20)	3.0 (20)	0.84 (16)	74	1150	—	2.28	684
4	1.0 (1)	1.0 (1)	0.31 (1)	83	1288	—	2.82	764
5	1.9 (1)	1.1 (1)	0.43 (20)	89	1376	0.22	1.91	704
6	0.9 (1)	0.9 (1)	0.41 (20)	85	1314	0.20	0.91	705
7	0.9 (1)	0.9 (1)	0.36 (20)	78	1196	0.20	0.92	706
8	3.7 (1)	6.3 (1)	0.34 (20)	78	1233	0.22	0.85	691

[I] Story level where this value was recorded.

REFERENCES

(1) Hanson, N. W. and Connor, H. W., "Seismic Resistance of Reinforced Concrete Beam-Column Joints," Proc. ASCE, Vol. 93, No. ST5, October 1967.

(2) Spencer, R. A., "Stiffness and Damping of Cyclically Loaded Prestressed Members," Presented at the 2nd Mexican Congress on Earthquake Engineering, Vera Cruz, May 1968.

(3) Lin, T. Y., "The Design of Prestressed Concrete Buildings for Earthquake Resistance," Proc. ASCE, Vol. 91, No. ST5, October 1965.

(4) Clough, R. W., King, I. P., and Wilson, E. L., "Large Capacity Multistory Frame Analysis Programs," Proc. ASCE, Vol. 89, No. ST4, August 1963.

(5) Giberson, M. F., "The Response of Nonlinear Multi-Story Structures Subjected to Earthquake Excitation," Ph. D. thesis, California Institute of Technology, May 1967.

(6) Jenschke, V. A., Clough, R. W. and Penzien, J., "Characteristics of Strong Ground Motion," Proc. 3rd World Conf. on Earthquake Engineering, New Zealand, 1965.

(7) Clough, R. W. and Benuska, K. L., "Nonlinear Earthquake Behavior of Tall Buildings," Proc. ASCE, Vol. 93, No. EM3, June 1967.

(8) "Uniform Building Code," Int. Conf. of Building Officials, Calif., 1964.

(9) "Uniform Building Code," Int. Conf. of Building Officials, Calif., 1967.

(10) Jennings, P. C., "Response of Simple Yielding Structures to Earthquake," Part II, Ph. D. thesis, California Institute of Technology, 1963.

(11) Giberson, op. cit., p. 139.

(12) Ibid., p. 140.

(13) United States Earthquakes 1933, USGS, pp. 64-65.

(14) United States Earthquakes 1952, USGS, pp. 87-89.

(15) Ibid., p. 79.

(16) Ibid., pp. 99-100.

APPENDIX A

Response Plots

In this appendix the variation of certain response parameters during the 8 seconds of earthquake excitation is shown graphically for the different structures. The plots for the horizontal forces acting at the 14th floor level show forces found using equation 28, the linear matrix equation of motion, and the inertia force is simply the mass times the absolute acceleration at the 14th floor level. The acceleration plots are all for absolute acceleration. The other parameters plotted are as defined in the text.

These time history plots further emphasize the effects, discussed in section 9, of variations in the assumed moment-rotation and damping properties. The very marked effect of including interfloor viscous damping can be seen by comparing the interstory drift and acceleration plots for structures 5 through 8 (which had $\xi_m = 0.01$ and $\xi_i = 0.02$) with those for structure 3 (which had $\xi_m = 0.01$ and $\xi_i = 0$). Acceleration records obtained for the upper floors of real structures during relatively small earthquakes (13, 14, 15, 16) suggest that the plots for structures 5 through 8 (as well as those for structures 2 and 4) are somewhat unrealistic, but the behaviour of the upper stories of real multistory structures during severe earthquakes is not yet well documented. However, the plots of the horizontal forces acting at the 14th floor level, which show that the force resulting from the interfloor viscous damping can be quite large relative to the inertia force, do appear to provide further evidence that this representation of structural damping is not wholly realistic.

These plots confirm that an accurate and realistic representation of structural damping is essential if reliable results are to be obtained from a dynamic structural analysis.

STRUCTURE 1 - INTERSTORY DRIFT AT VARIOUS FLOOR LEVELS (INS)

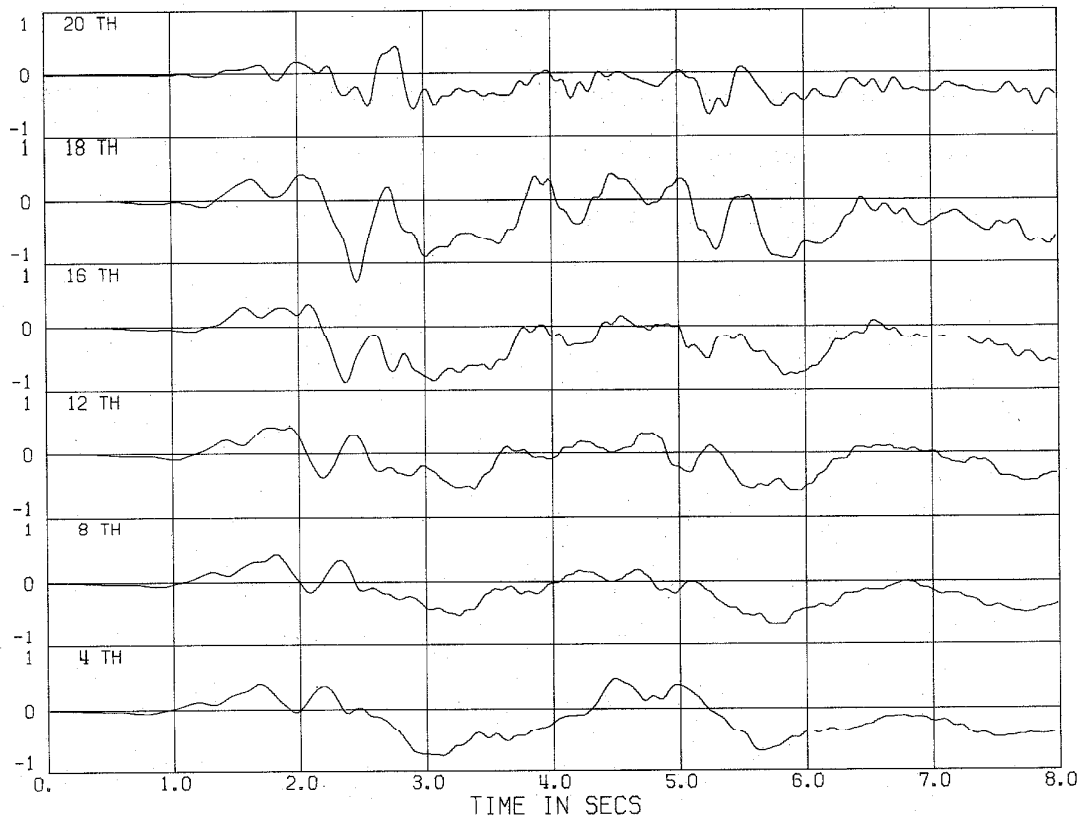

STRUCTURE 2 - INTERSTORY DRIFT AT VARIOUS FLOOR LEVELS (INS)

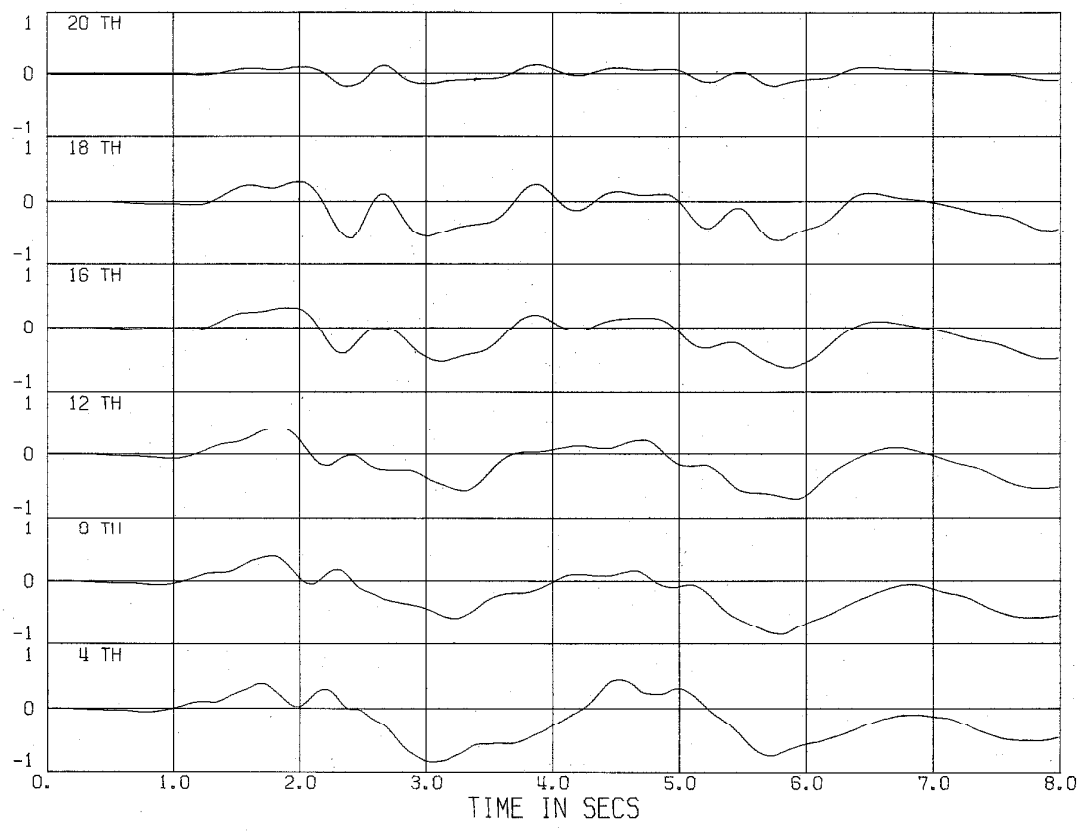

STRUCTURE 3 - INTERSTORY DRIFT AT VARIOUS FLOOR LEVELS (INS)

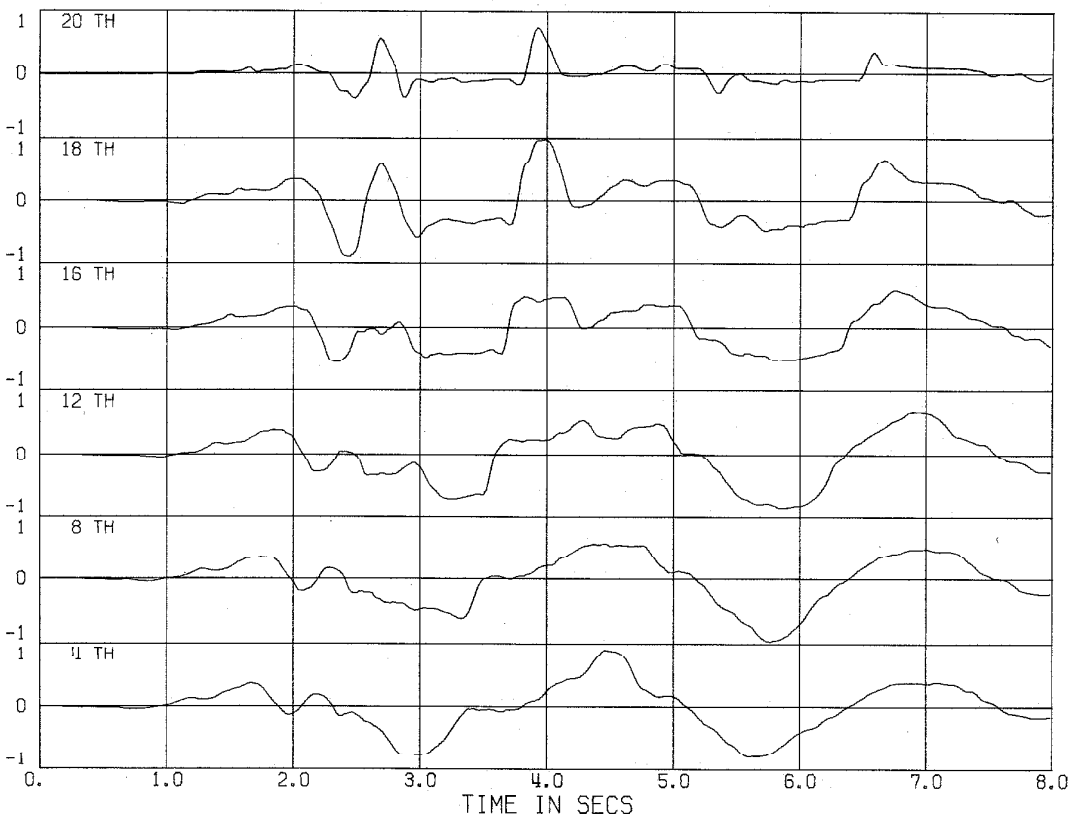

STRUCTURE 4 - INTERSTORY DRIFT AT VARIOUS FLOOR LEVELS (INS)

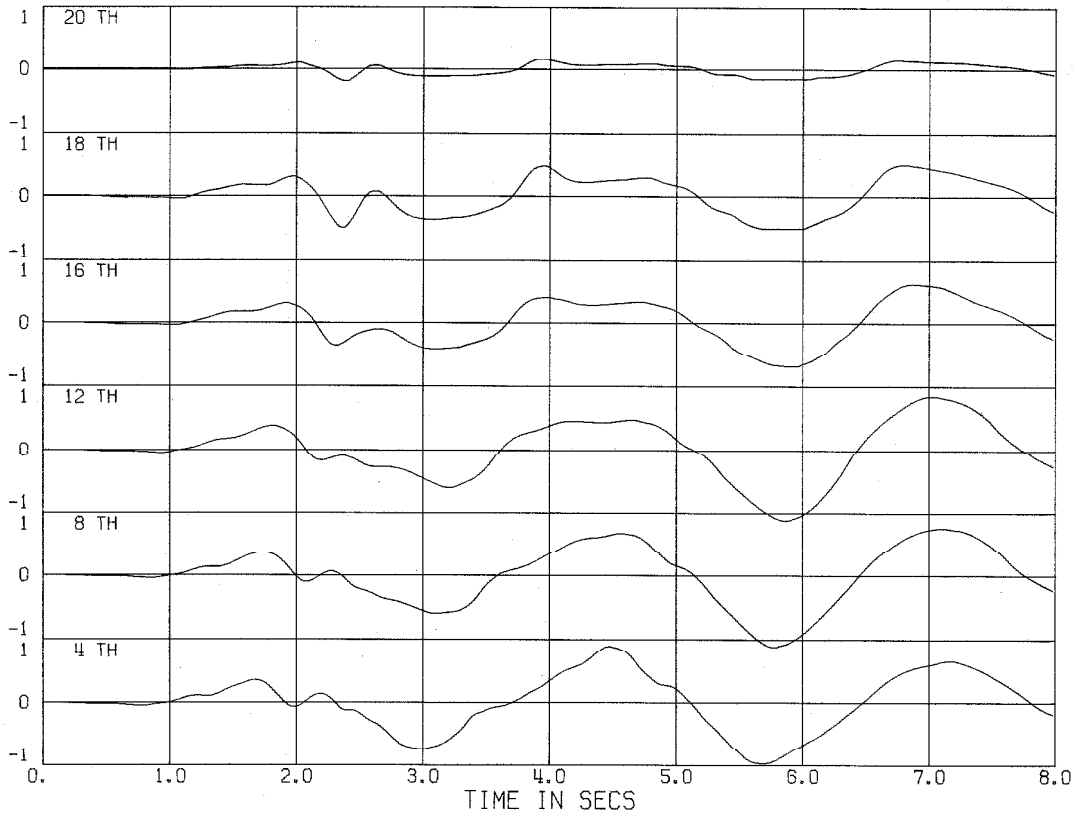

STRUCTURE 5 - INTERSTORY DRIFT AT VARIOUS FLOOR LEVELS (INS)

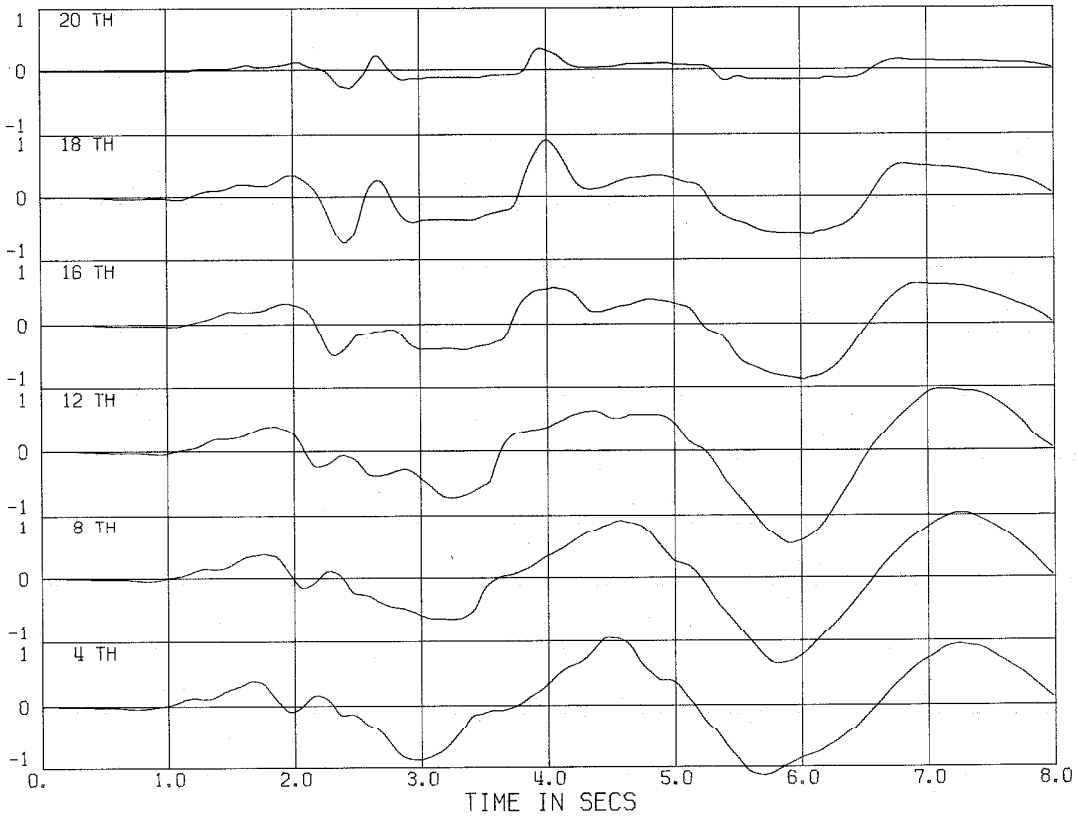

STRUCTURE 6 - INTERSTORY DRIFT AT VARIOUS FLOOR LEVELS (INS)

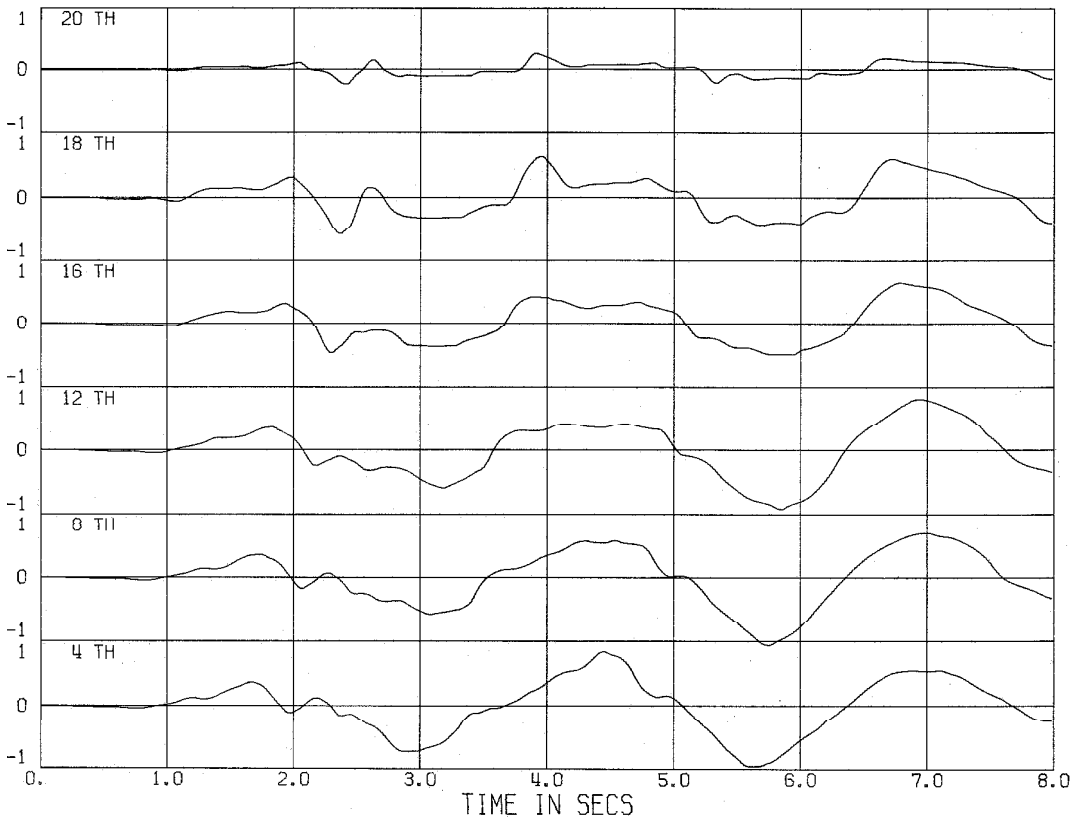

STRUCTURE 7 - INTERSTORY DRIFT AT VARIOUS FLOOR LEVELS (INS)

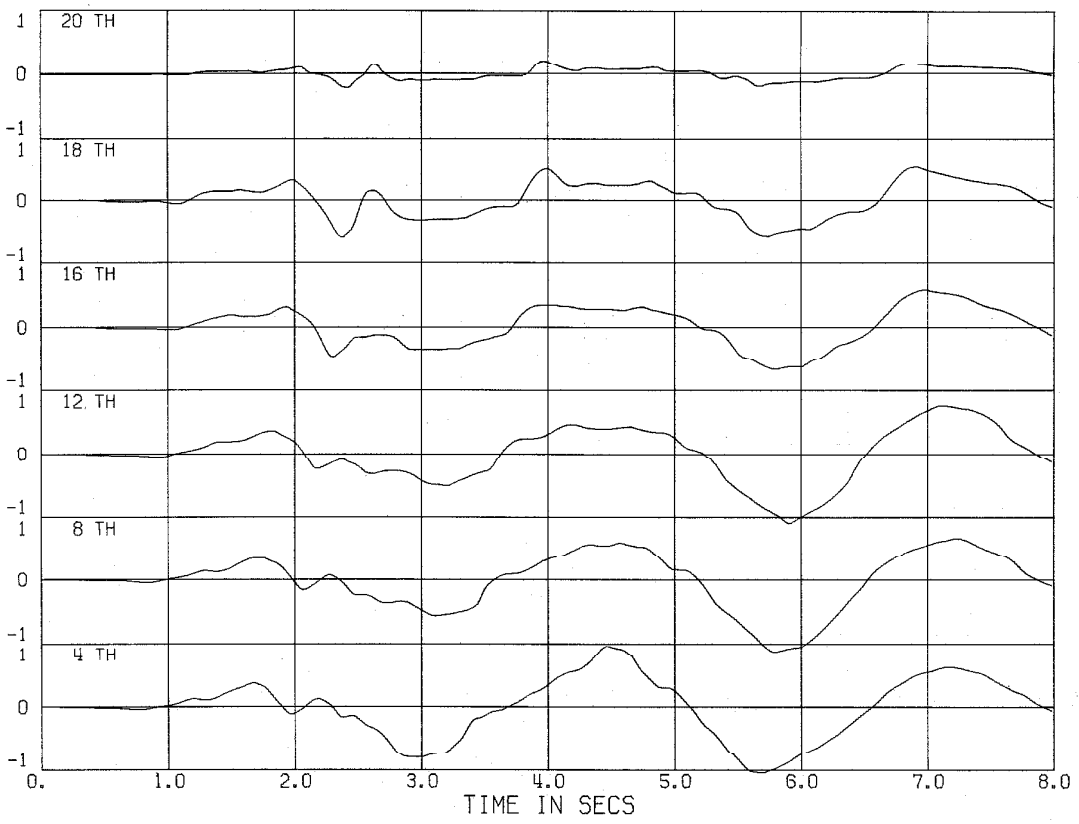

STRUCTURE 8 - INTERSTORY DRIFT AT VARIOUS FLOOR LEVELS (INS)

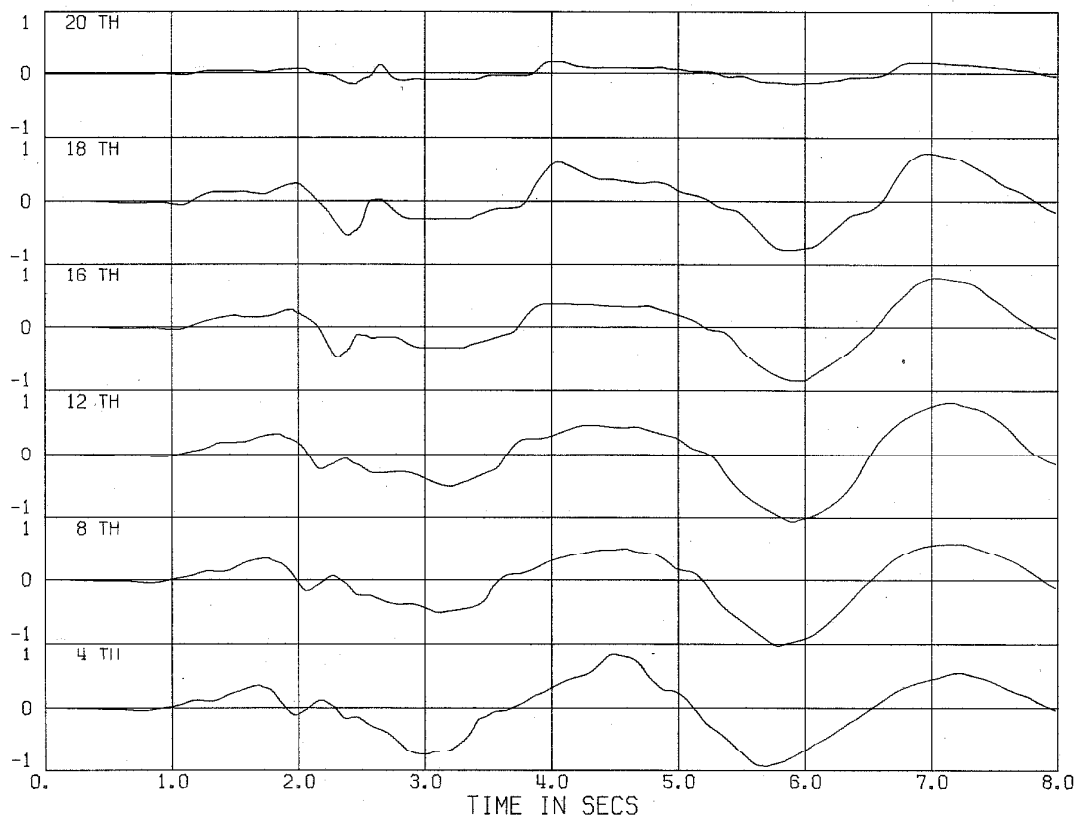

STRUCTURE 1 - ACCEL AT VARIOUS FLOOR LEVELS (FRAC. OF G)

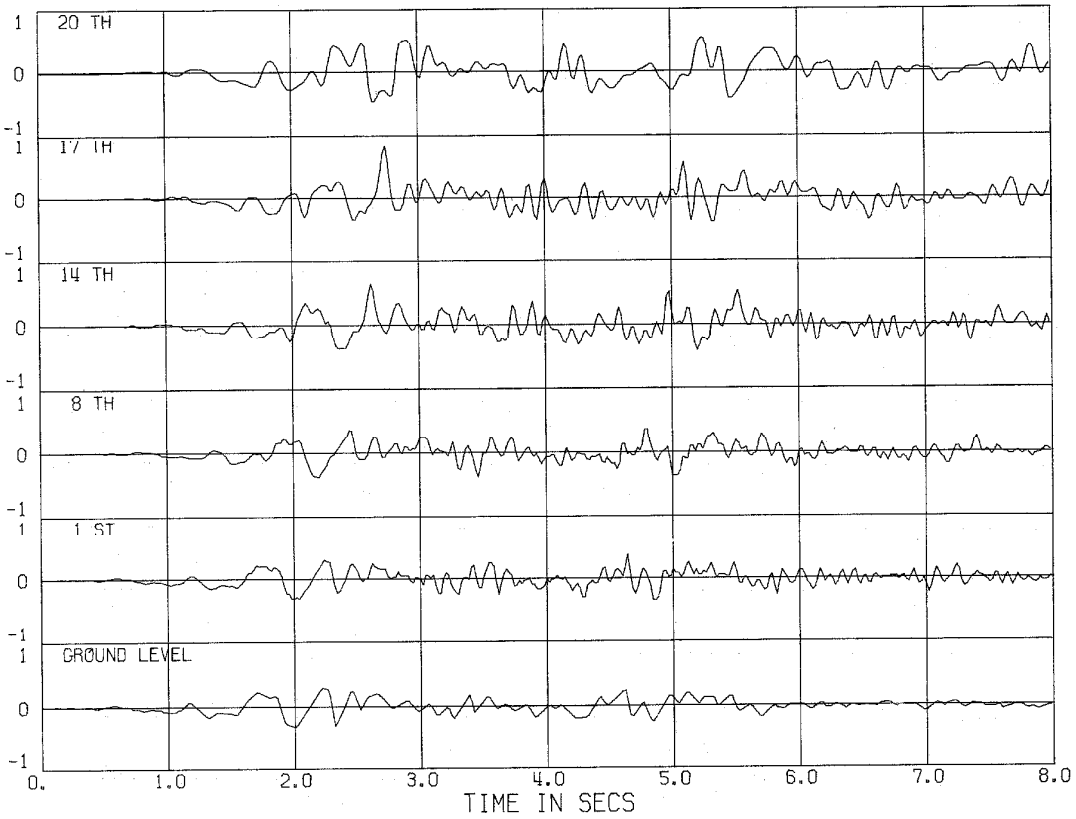

STRUCTURE 2 - ACCEL AT VARIOUS FLOOR LEVELS (FRAC. OF G)

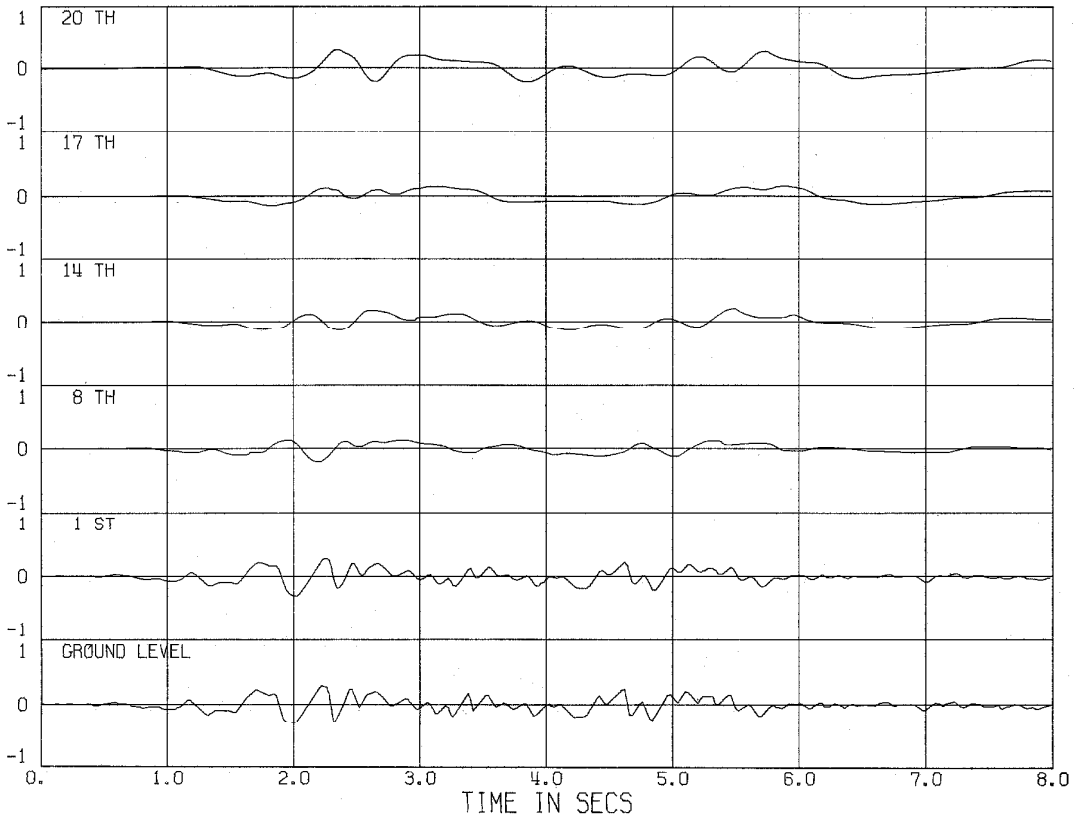

STRUCTURE 3 - ACCEL AT VARIOUS FLOOR LEVELS (FRAC. OF G)

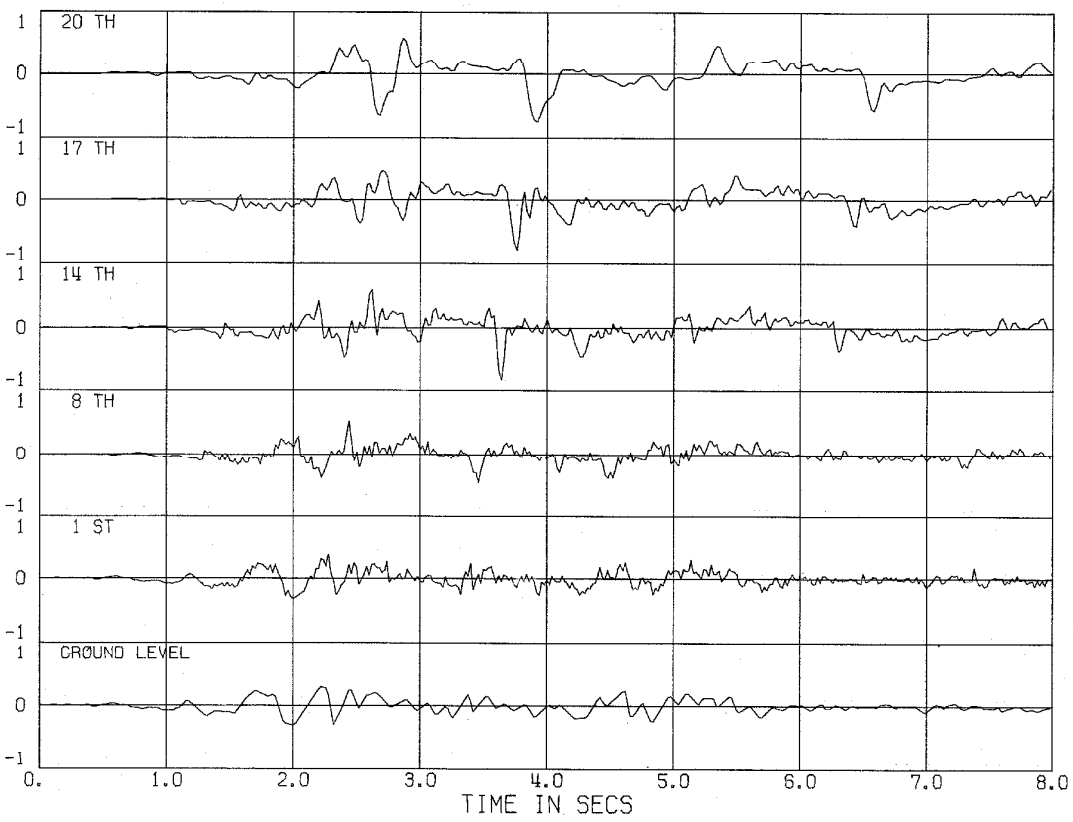

STRUCTURE 4 - ACCEL AT VARIOUS FLOOR LEVELS (FRAC. OF G)

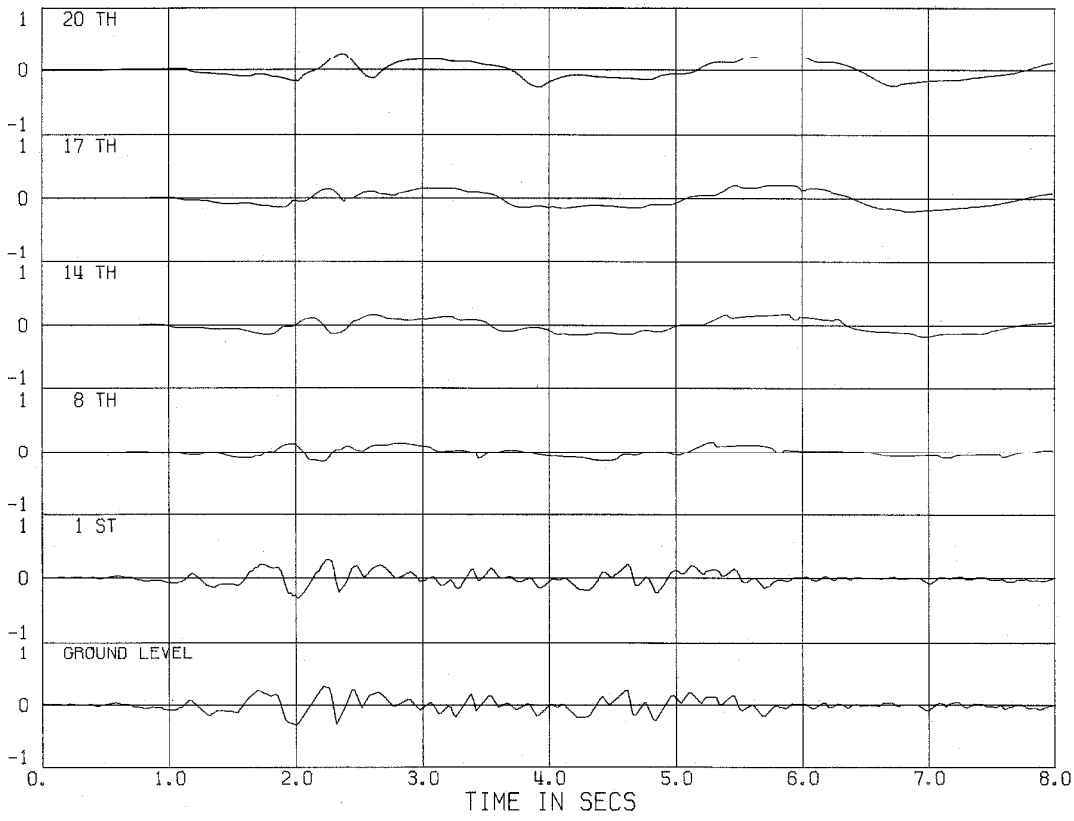

STRUCTURE 5 - ACCEL AT VARIOUS FLOOR LEVELS (FRAC. OF G)

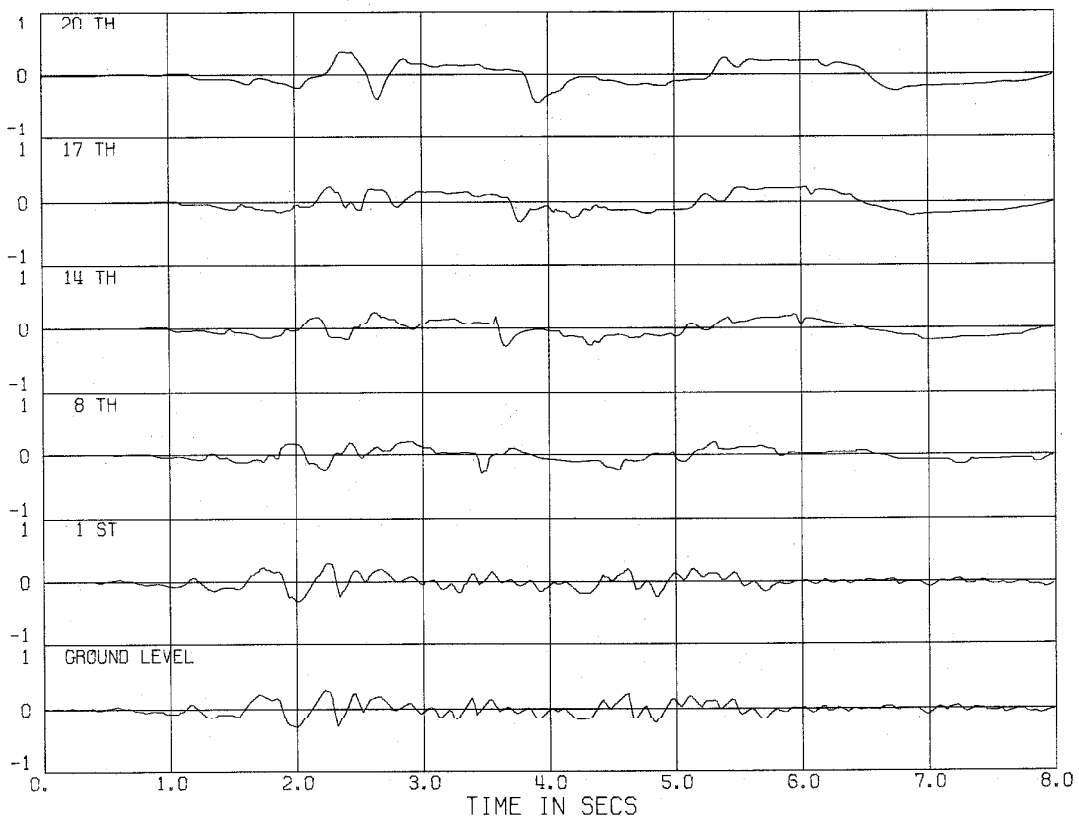

STRUCTURE 6 - ACCEL AT VARIOUS FLOOR LEVELS (FRAC. OF G)

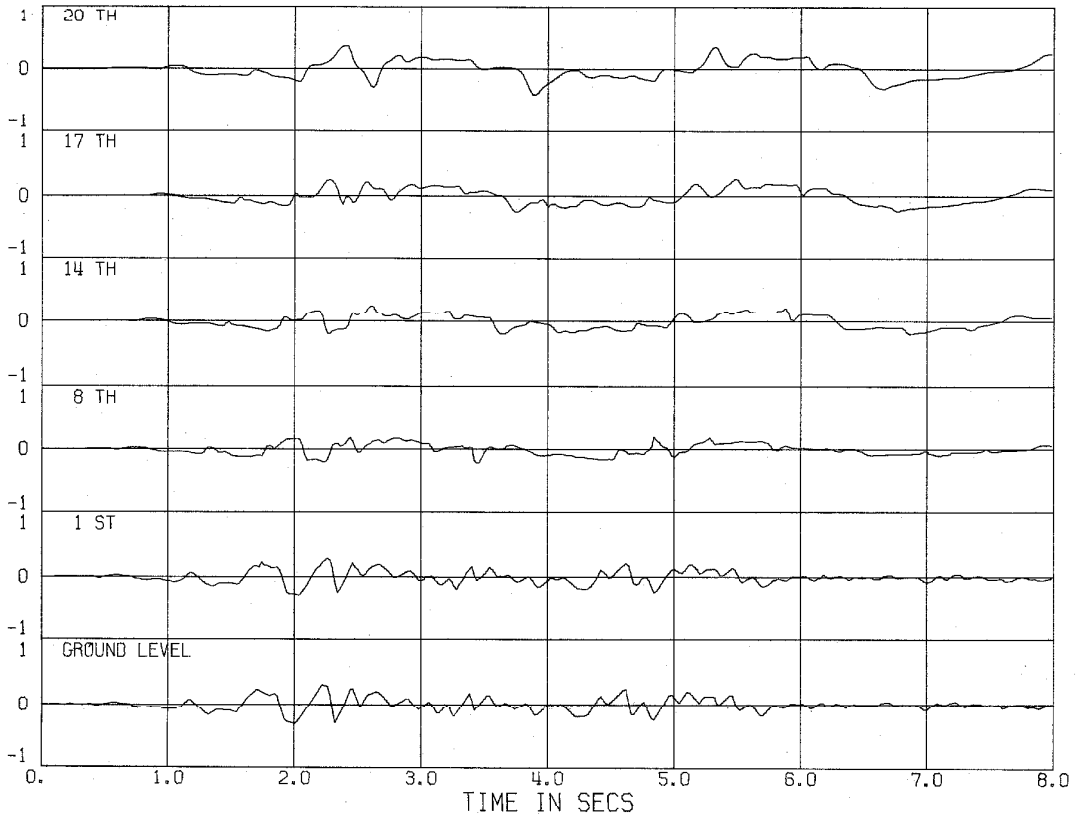

STRUCTURE 7 - ACCEL AT VARIOUS FLOOR LEVELS (FRAC. OF G)

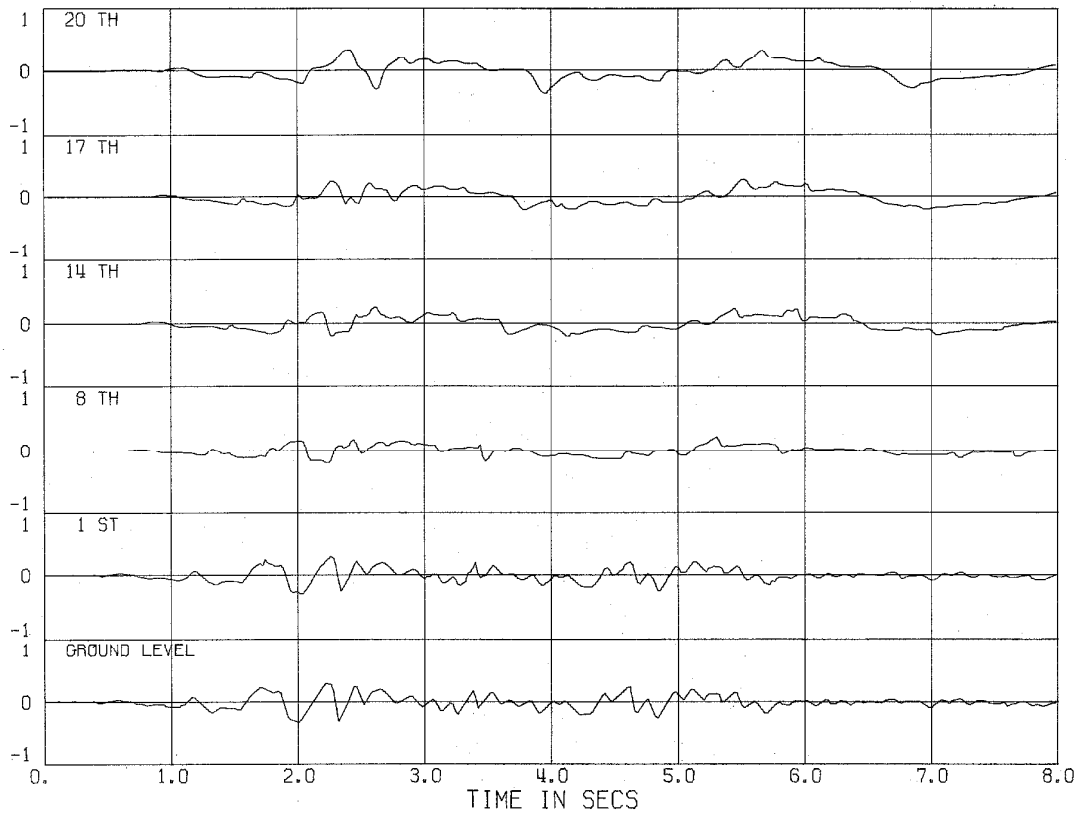

STRUCTURE 8 - ACCEL AT VARIOUS FLOOR LEVELS (FRAC. OF G)

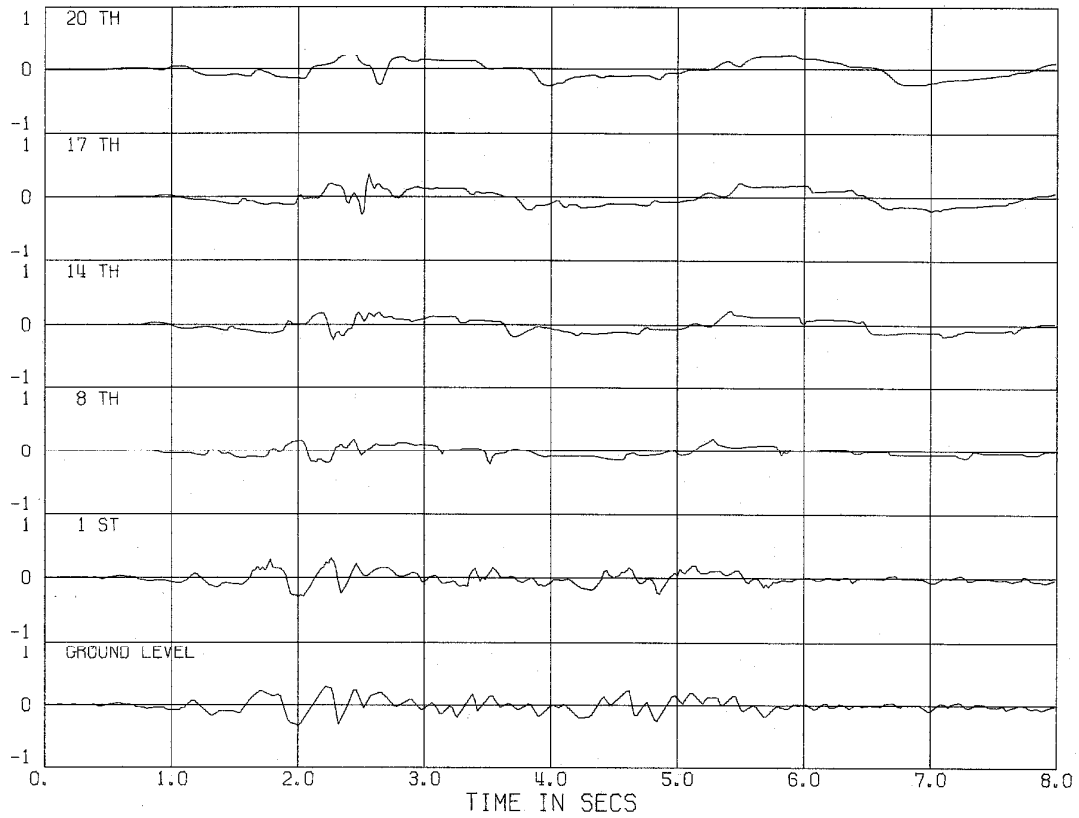

STRUCTURE 1 - HORIZONTAL FORCES ACTING AT 14TH FLOOR LEVEL

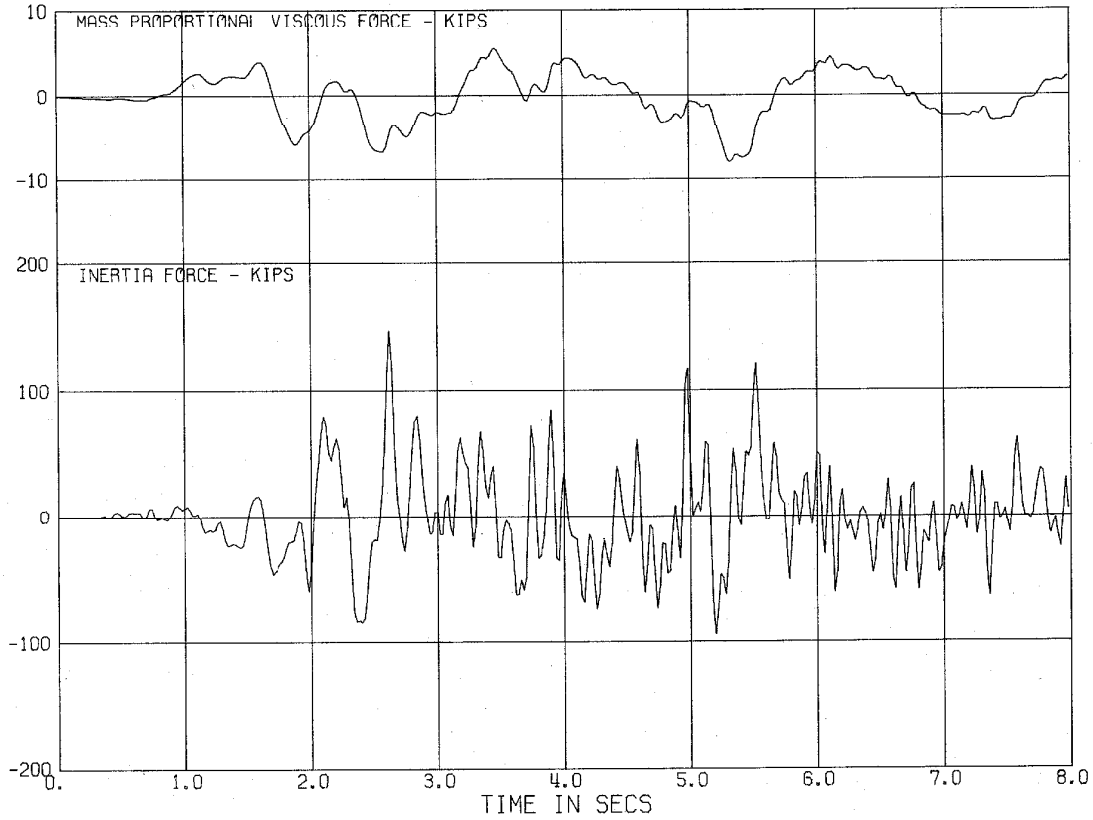

STRUCTURE 2 - HORIZONTAL FORCES ACTING AT 14TH FLOOR LEVEL

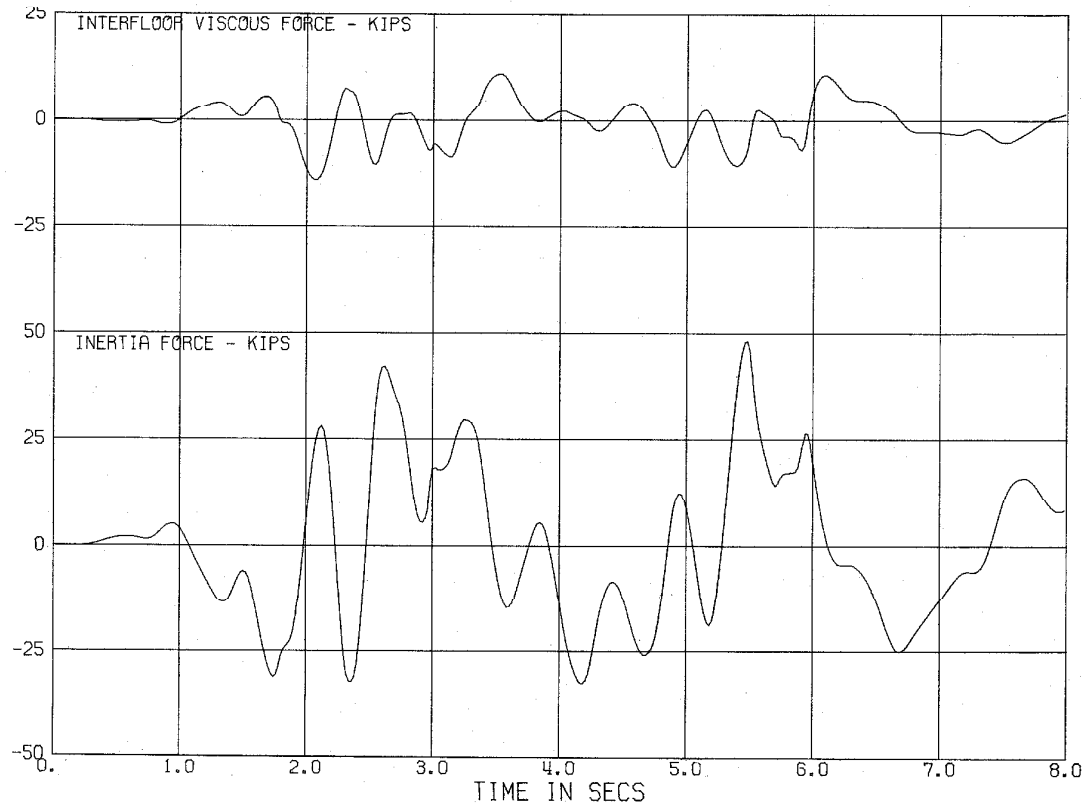

STRUCTURE 3 - HORIZONTAL FORCES ACTING AT 14TH FLOOR LEVEL

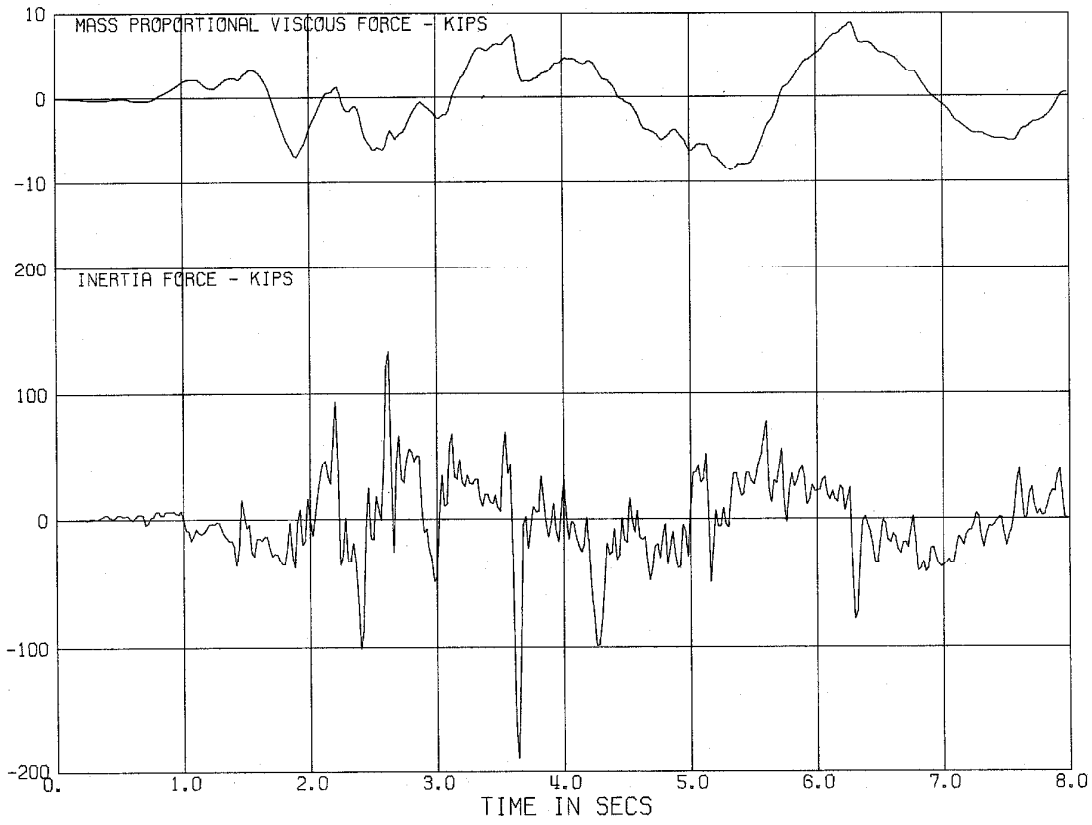

STRUCTURE 4 - HORIZONTAL FORCES ACTING AT 14TH FLOOR LEVEL

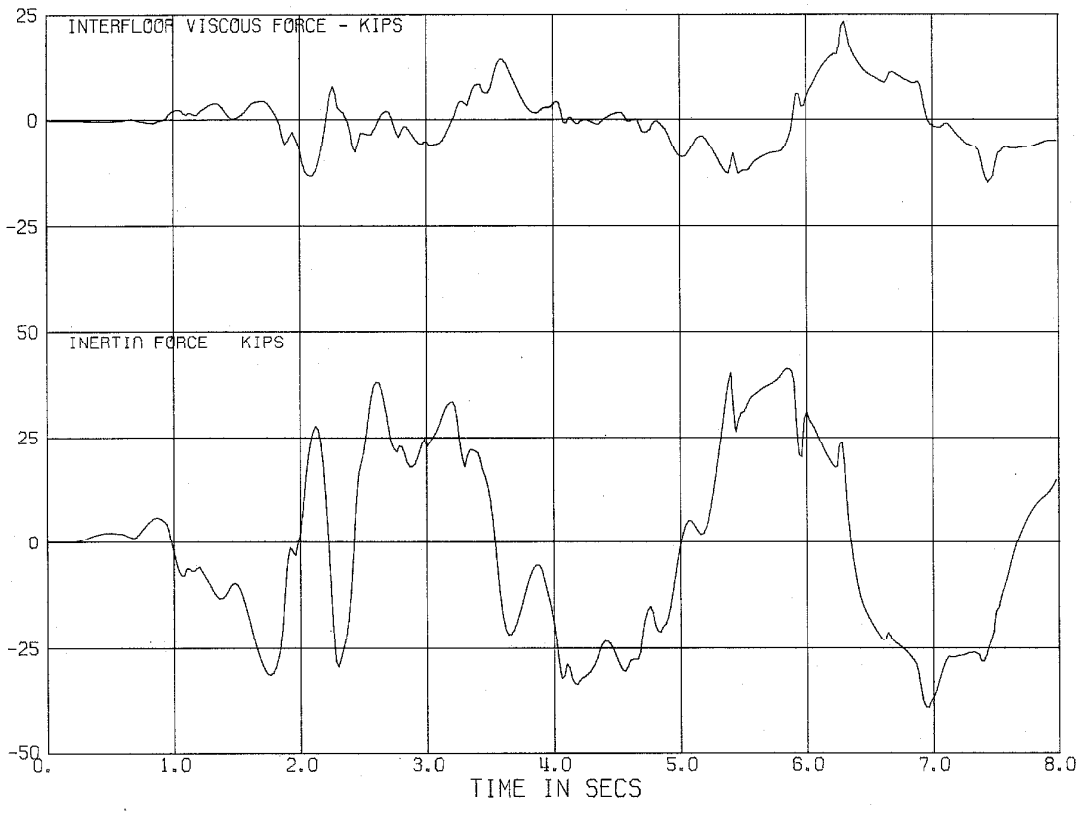

STRUCTURE 5 - HORIZONTAL FORCES ACTING AT 14TH FLOOR LEVEL

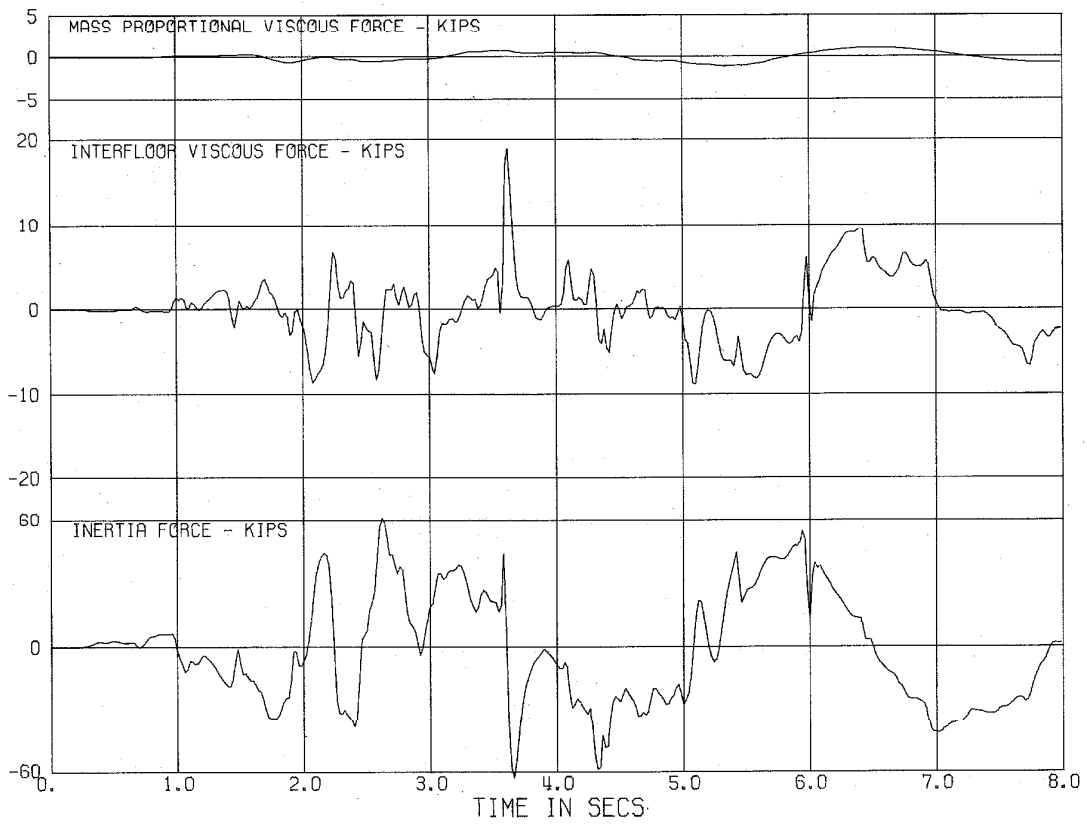

STRUCTURE 6 - HORIZONTAL FORCES ACTING AT 14TH FLOOR LEVEL

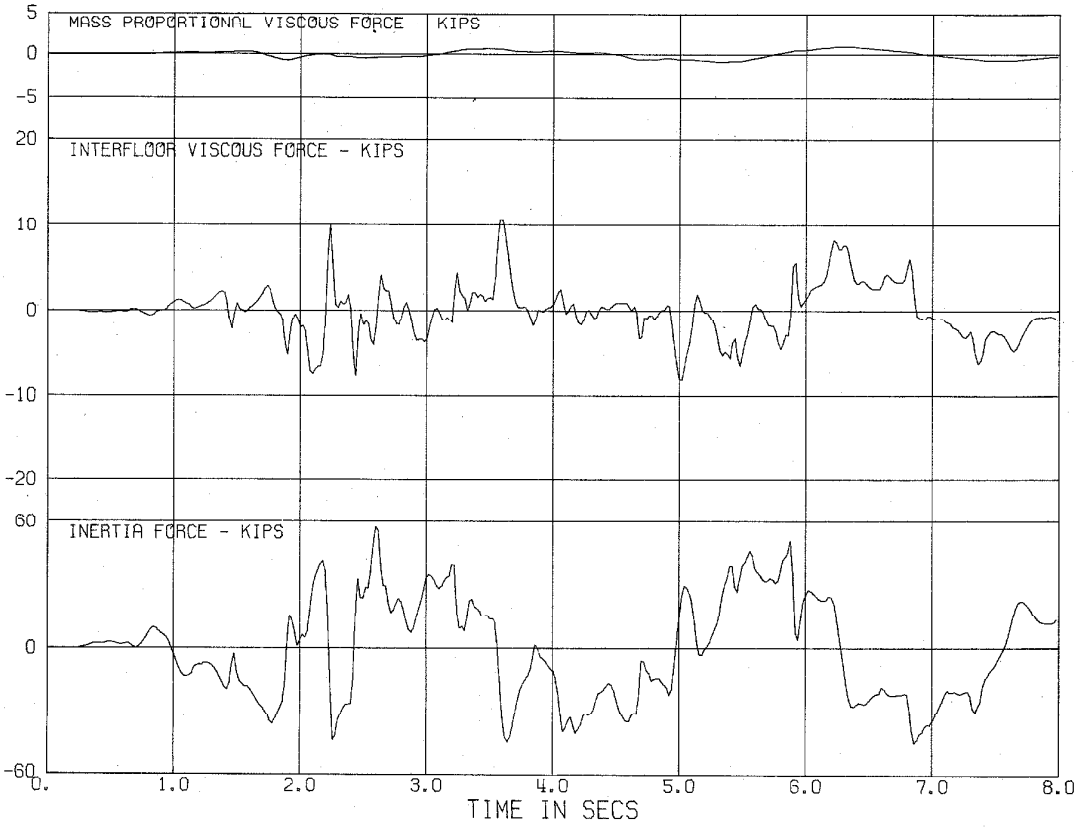

STRUCTURE 7 - HORIZONTAL FORCES ACTING AT 14TH FLOOR LEVEL

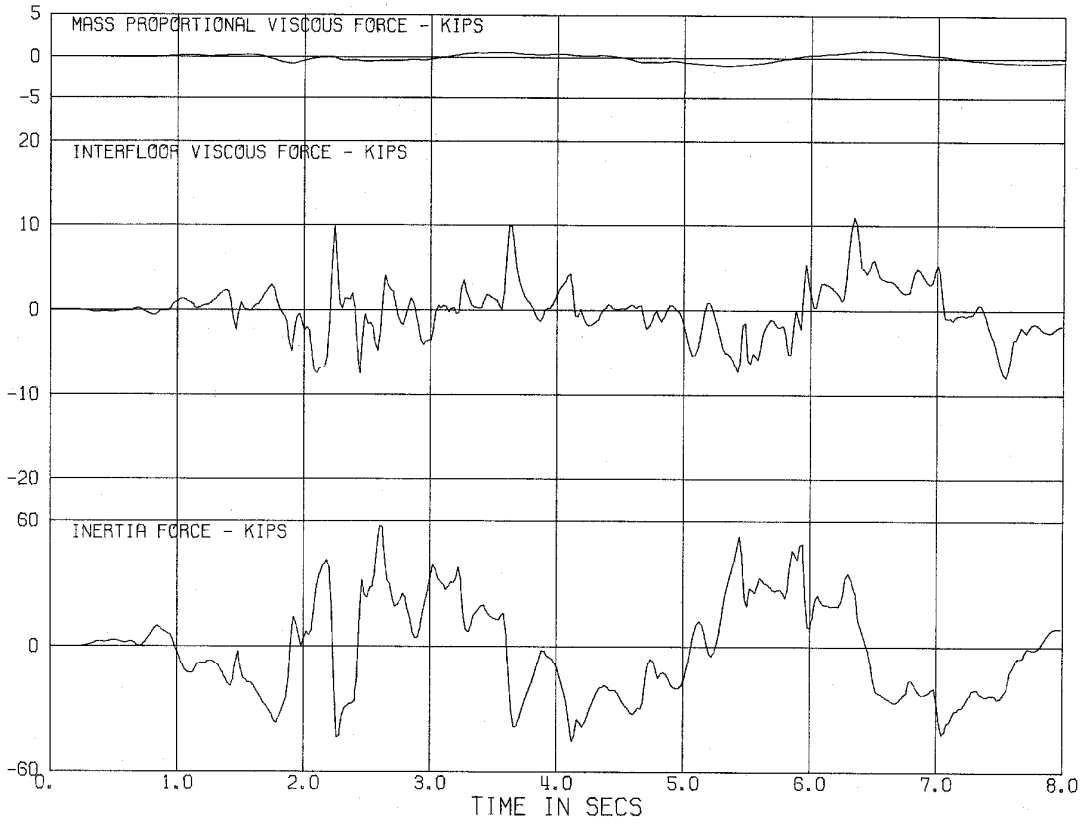

STRUCTURE 8 - HORIZONTAL FORCES ACTING AT 14TH FLOOR LEVEL

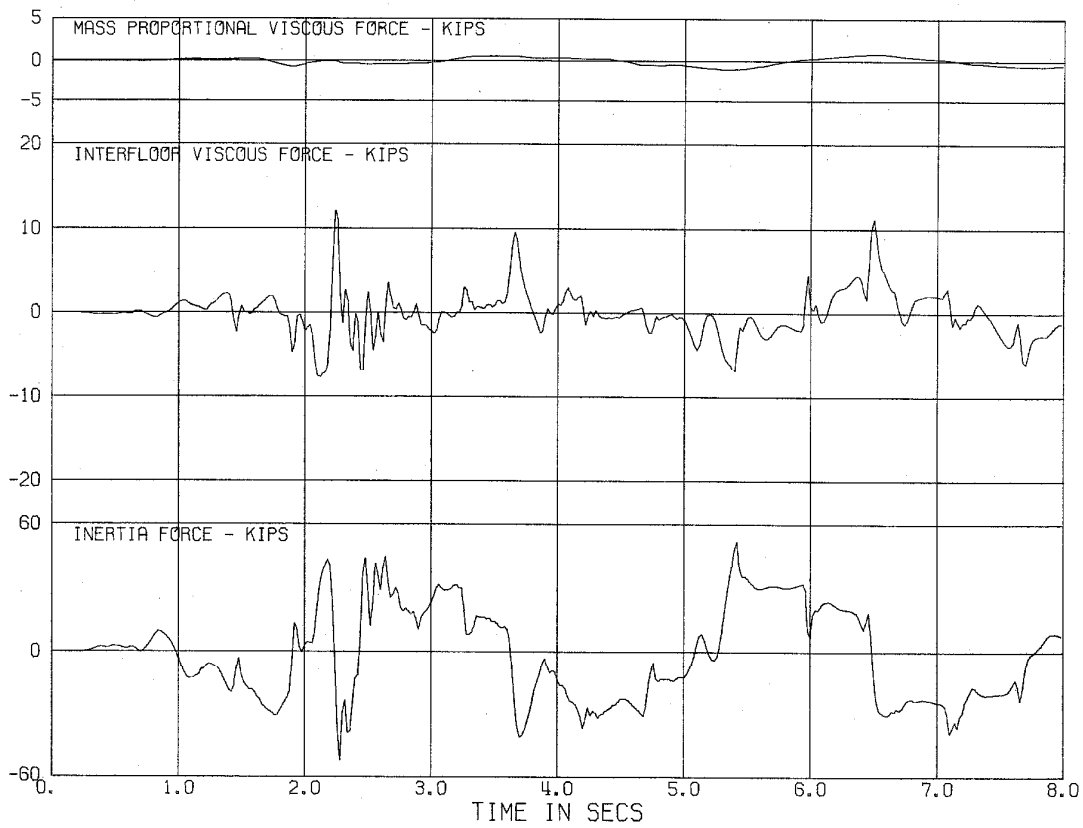

APPENDIX B

Comparison of Elastic and Nonlinear Response

The responses of one elastic and one elasto-plastic version of the basic 20 story structure (designated A20/2.2/2/6 by Giberson (5)) to the accelerograms of the North-South component of the El Centro 1940 earthquake record and the eight Jennings Pseudo-earthquakes (10) (adjusted so that the r.m.s. value of each accelerogram is approximately 1.2 times that of the El Centro record (11)), were found. Both versions of the structure had the same viscous damping, with $\xi_m = 0.1$ and $\xi_i = 0$. The elasto-plastic version had $p = 0.05$, and for the elastic version p was of course taken as 1. Girder and column yield strengths for the elasto-plastic version were respectively twice and six times the design strengths. Some of the response results discussed here for the elasto-plastic version of the structure are those found by Giberson (12).

The results given in Tables B1 and B2 show that the effect on displacement of changing the structural properties from elastic to elasto-plastic is not great. The maximum recorded displacements of the 20th floor, and the maximum recorded interstory drifts, show random variations with the different earthquakes for both versions of the structure. The maximum displacements found from the elastic analyses were generally greater than those found from the nonlinear analyses, but for pseudo-earthquakes 3 and 8 they were less. It appears that either an elastic or a nonlinear analysis could be used to find approximate values of the maximum displacements of this structure resulting from earthquake excitation.

Tables B1 and B2 show that for any of the earthquakes, the maximum recorded absolute story acceleration found by the nonlinear analysis is significantly less than that found by the elastic analysis. The maximum ductility factors (which for the elastic version of the structure are simply the ratio of the maximum recorded end moment in a member to the yield moment for the same member in the elasto-plastic version) also indicate significant differences in the way the two versions of the structure deformed. Nonlinear deformations in the girders of the elasto-plastic version, which occurred at all story levels, apparently reduced the deformations in the exterior columns compared to those in the elastic version.

From this comparison it appears that expected displacements for a real structure might be judged from an elastic analysis, but story accelerations and the deformations of individual members, both of which can be structurally significant, can only be assessed from a nonlinear analysis. It should be noted that for the particular structure considered, there was very little yielding in the columns of the elasto-plastic version. What little yielding did occur was confined to the interior columns of the upper few stories. Greater differences might be observed between the responses of elastic and elasto-plastic versions of structures in which more yielding of the columns occurs.

Table B1: Comparison of Elastic and Elasto-plastic Response Results

Earthquake	Maximum Displacement (20th Floor)	Maximum Interstory Drift	Maximum Absolute Acceleration	Maximum Ductility Factors			Type of Structure
				All Girders	Interior Columns	Exterior Columns	
El Centro NS (1940)	13.82 in. 11.52 in.	1.65 in. 1.29 in.	1.34 g 0.81 g	4.27 4.44	3.51 2.99	1.87 0.83	Elastic Elasto-plastic
Pseudo Earthquake 1	9.47 in. 8.98 in.	1.02 in. 0.98 in.	0.70 g 0.47 g	2.56 3.58	1.91 1.74	1.12 0.71	Elastic Elasto-plastic
" 2	14.44 in. 14.43 in.	1.47 in. 1.31 in.	0.93 g 0.49 g	3.65 5.00	2.46 3.11	1.56 0.81	Elastic Elasto-plastic
" 3	8.90 in. 9.92 in.	0.97 in. 1.24 in.	0.74 g 0.53 g	2.01 4.63	1.94 1.47	1.08 0.80	Elastic Elasto-plastic
" 4	14.06 in. 10.96 in.	1.32 in. 0.93 in.	0.89 g 0.54 g	3.50 3.96	2.45 2.02	1.60 0.80	Elastic Elasto-plastic
" 5	13.84 in. 9.69 in.	1.20 in. 0.91 in.	0.77 g 0.53 g	3.09 3.63	2.08 2.28	1.29 0.76	Elastic Elasto-plastic
" 6	10.80 in. 8.91 in.	1.08 in. 0.99 in.	0.78 g 0.56 g	2.72 4.01	1.76 2.58	1.13 0.78	Elastic Elasto-plastic
" 7	10.47 in. 8.52 in.	1.18 in. 0.97 in.	0.86 g 0.49 g	2.96 3.75	2.32 2.53	1.42 0.79	Elastic Elasto-plastic
" 8	9.64 in. 10.13 in.	1.10 in. 1.14 in.	0.78 g 0.50 g	2.38 4.36	2.08 1.23	1.19 0.77	Elastic Elasto-plastic

Table B2: Mean Values and Spread of Displacement and Acceleration Results for Eight Pseudo-Earthquakes

	Elastic		Elasto-plastic	
	Mean	Spread	Mean	Spread
Maximum Displacement (20th Floor)	11.95 in.	5.54 in.	10.19 in.	5.91 in.
Maximum Interstory Drift	1.17 in.	0.50 in.	1.08 in.	0.40 in.
Maximum Absolute Acceleration	0.81 g	0.23 g	0.51 g	0.09 g